



▼ Searched ▼

Cite

▼ Full Text ▼



Citation Count

Related Citations

Altmetric Journal FComme

▼ Share ▼ Note



Cannabidiol sensitizes TRPV2 channels to activation by 2-APB

The cation-permeable TRPV2 channel is essential for cardiac and immune cells.

[View original](#)

This is a preprint.

It has not yet been peer reviewed by a journal.

>

The National Library of Medicine is [running a pilot](#) to include preprints that result from research funded by NIH in PMC and PubMed.

Aaron Gochman

²Molecular Physiology and Biophysics Section, Porter Neuroscience Research Center, National Institute of Neurological Disorders and Stroke, National Institutes of Health, Bethesda, MD, 20892 USA

³Current affiliation: Vanderbilt University School of Medicine, Nashville, TN 37232, USA

Xiaofeng Tan

²Molecular Physiology and Biophysics Section, Porter Neuroscience Research Center, National Institute of Neurological Disorders and Stroke, National Institutes

of Health, Bethesda, MD, 20892 USA

Chanhung Bae

²Molecular Physiology and Biophysics Section, Porter Neuroscience Research Center, National Institute of Neurological Disorders and Stroke, National Institutes of Health, Bethesda, MD, 20892 USA

⁴Current affiliation: Janssen R&D, Biologics Discovery, Spring House, PA, USA.

Helen Chen

¹Department of Molecular Biosciences, College of Natural Sciences, The University of Texas at Austin, TX, 78712 USA.

Kenton J. Swartz

²Molecular Physiology and Biophysics Section, Porter Neuroscience Research Center, National Institute of Neurological Disorders and Stroke, National Institutes of Health, Bethesda, MD, 20892 USA

Andrés Jara-Oseguera

¹Department of Molecular Biosciences, College of Natural Sciences, The University of Texas at Austin, TX, 78712 USA.

¹Department of Molecular Biosciences, College of Natural Sciences, The University of Texas at Austin, TX, 78712 USA.

²Molecular Physiology and Biophysics Section, Porter Neuroscience Research Center, National Institute of Neurological Disorders and Stroke, National Institutes of Health, Bethesda, MD, 20892 USA

³Current affiliation: Vanderbilt University School of Medicine, Nashville, TN 37232, USA

⁴Current affiliation: Janssen R&D, Biologics Discovery, Spring House, PA, USA.

¶Equal contributors

Contributed by

Author contributions

AG (Conceptualization, Methodology, Validation, Formal Analysis, Investigation, Data Curation, Writing – Original Draft Preparation, Writing - Review & Editing, Visualization), XT (Methodology, Validation, Formal Analysis, Investigation, Data Curation, Writing – Original Draft Preparation, Writing - Review & Editing, Visualization), CB (Methodology, Investigation), HC (Methodology, Investigation), KJS (Writing - Review & Editing, Funding Acquisition), AJO (Conceptualization, Methodology, Validation, Formal Analysis, Investigation, Data Curation, Writing – Original Draft Preparation, Writing - Review & Editing, Visualization, Supervision, Project Administration, Funding Acquisition).

The complete version history of this preprint is available at [bioRxiv](#).

Associated Data

[Supplementary Materials](#)

[Data Availability Statement](#)

All data needed to evaluate the conclusions in the paper are present in the paper, the Supplementary Materials, or uploaded as Source data. Maps for conformations A and B for rTRPV2 have been deposited in the Electron Microscopy Data Bank (EMDB) under accession codes EMD-29526 and EMD-29532, respectively. Models of conformations A and B for rTRPV2 have been deposited in the Protein Data Bank with accession codes 8FX8 and 8FXG, respectively.

Abstract

The cation-permeable TRPV2 channel is essential for cardiac and immune cells. Cannabidiol (CBD), a non-psychoactive cannabinoid of clinical relevance, is one of the few molecules known to activate TRPV2. Using the patch-clamp technique we discover that CBD can sensitize current responses of the rat TRPV2 channel to the synthetic agonist 2-aminoethoxydiphenyl borate (2-APB) by over two orders of magnitude, without sensitizing channels to activation by moderate (40 °C) heat. Using cryo-EM we uncover a new small-molecule binding site in the pore domain of rTRPV2 that can be

occupied by CBD in addition to a nearby CBD site that had already been reported. The TRPV1 and TRPV3 channels share >40% sequence identity with TRPV2 are also activated by 2-APB and CBD, but we only find a strong sensitizing effect of CBD on the response of mouse TRPV3 to 2-APB. Mutations at non-conserved positions between rTRPV2 and rTRPV1 in either the pore domain or the CBD sites failed to confer strong sensitization by CBD in mutant rTRPV1 channels. Together, our results indicate that CBD-dependent sensitization of TRPV2 channels engages multiple channel regions and possibly involves more than one CBD and 2-APB sites. The remarkably robust effect of CBD on TRPV2 and TRPV3 channels offers a promising new tool to both understand and overcome one of the major roadblocks in the study of these channels – their resilience to activation.

Keywords: TRPV1, TRPV3, gating, sensitization, potentiation, cannabinoids

Introduction

The non-selective, cation-permeable Transient Receptor Potential Vanilloid 2 (TRPV2) channel is a homo-tetrameric protein ([Huynh et al., 2016](#); [Zubcevic et al., 2016](#)) expressed in multiple cell types and tissues in animals ([Caterina et al., 1999](#); [Tamura et al., 2005](#)). Adult mice in which TRPV2 channel expression in cardiomyocytes was ablated died within two weeks and exhibited severe structural abnormalities of the heart,

and TRPV2-deficient cardiomyocytes from neonatal

mice were also highly dysfunctional after growth in culture ([Katanosaka et al., 2014](#)), indicating that TRPV2 channel expression in cardiomyocytes is required for normal development and function of the heart ([Katanosaka et al., 2014; Iwata and Matsumura, 2019](#)). In macrophages, TRPV2 channel expression is essential for phagocytosis ([Link et al., 2010; Lévêque et al., 2018](#)), in pancreatic β-cells it influences insulin secretion ([Hisanaga et al., 2009](#)), in red blood cells it contributes to their response to osmotic challenges ([Belkacemi et al., 2021](#)), and its expression levels are significantly altered in multiple types of cancers ([Monet et al., 2010; Yamada et al., 2010; Kudou et al., 2019; Siveen et al., 2020; Guéguinou et al., 2021](#)).

Interestingly, the identity of the stimuli that orchestrate TRPV2 channel activity in each of the examples mentioned above remain unknown. Very few stimuli capable of activating the TRPV2 channel have been identified; the extreme temperatures (> 55°C) required to activate rodent TRPV2 channels ([Caterina et al., 1999; Tamura et al., 2005; Yao et al., 2011; Liu and Qin, 2016](#)) and the complete lack of thermo-sensitivity of the human orthologue under basal conditions ([Neeper et al., 2007; Yao et al., 2011](#)) exclude a likely role for this protein in thermo-detection. Yet, oxidative modification of specific methionine residues in rodent and human

TRPV2 channels resulted in robust channel activation

at much lower temperatures ([Fricke et al., 2019](#)), suggesting that redox processes, temperature, and membrane depolarization together could promote channel activity in native tissues under physiological conditions. The synthetic agonist 2-aminoethoxydiphenyl borate (2-APB) robustly activates rodent but not human TRPV2 channels ([Hu et al., 2004](#); [Juvin et al., 2007](#)), and even rodent TRPV2 channels have very low apparent affinity for 2-APB, with an $EC_{50} > 1$ mM ([Gao et al., 2016a](#); [Liu and Qin, 2016](#)) that is close to the solubility limit of the compound. Importantly, 2-APB also targets other channels, including TRP channels ([Hu et al., 2004](#); [Xu et al., 2005](#); [Togashi et al., 2008](#); [Kovacs et al., 2012](#)), STIM-Orai channels ([Bootman et al., 2002](#)) and gap-junctions ([Bai et al., 2006](#)). Cannabidiol (CBD), a non-psychotropic compound from the cannabis plant that has received much attention recently for its potential use in treating a variety of disorders ([Pauli et al., 2020](#)) has also been found to activate rodent TRPV2 channels with much higher apparent affinity than 2-APB ([Qin et al., 2008](#)). Other cannabis-derived compounds, including Δ^9 -tetrahydrocannabinol (THC), are also reported to activate TRPV2 channels ([Neeper et al., 2007](#); [Qin et al., 2008](#); [Zhang et al., 2022](#)).

In stark contrast with the limited number of stimuli that activate the TRPV2 channel, the TRPV1 channel

expressed in nociceptive neurons can be activated by the stimuli that activate the TRPV2 channel, but also by a remarkably diverse set of inflammatory mediators ([Zygmunt et al., 1999](#); [Hwang et al., 2000](#); [Shin et al., 2002](#); [Nieto-Posadas et al., 2011](#); [Joseph et al., 2019](#)), animal toxins ([Bohlen et al., 2010](#); [Yang et al., 2015](#)) and natural products ([Caterina et al., 1997](#); [Salazar et al., 2008](#)). Paradoxically, both channels are >40% identical in amino acid sequence, have an identical structural fold ([Gao et al., 2016b](#); [Huynh et al., 2016](#); [Zubcevic et al., 2016](#)), and utilize similar mechanisms to gate the passage of cations through their ion conduction pathway in response to stimulation with 2-APB ([Jara-Oseguera et al., 2019](#)). Notably, high-sensitivity to a TRPV1-specific agonist, resiniferatoxin (RTx), could be engineered into the rat TRPV2 channel simply by substituting four non-conserved residues in the binding site with the residues at structurally equivalent positions in the TRPV1 channel ([Yang et al., 2016](#); [Zhang et al., 2016, 2019](#)). These findings highlight the mechanistic similarities that exist between the two channels even though they are so differently poised for activation.

Cryo-electron microscopy (cryo-EM) structures of rat TRPV2 channels obtained in the presence of CBD ([Pumroy et al., 2019](#)) and CBD together with 2-APB ([Pumroy et al., 2022](#)) suggest that the cannabinoid binds close to the regions in the channel that directly gate the passage of cations through the pore in response to

stimulation. Here we set out to use the patch clamp technique and cryo-EM structural determination to characterize the actions of CBD on rat TRPV2 channels, and learn more about the mechanisms of TRPV2 channel activation. We discovered that CBD potently sensitizes the rTRPV2 channel to activation by 2-APB, without an effect on channel sensitivity to moderate heat. We obtained structures of rTRPV2 in the presence of CBD and 2-APB representing two non-conducting conformations; one has CBD bound to a previously identified site ([Pumroy et al., 2019, 2022](#)) providing confirmatory evidence for the site. The other conformation exhibits an additional CBD molecule bound to a new site located nearby the S5 and S6 helices and the S4-S5 linker, which adopts a different conformation stabilizing the second bound CBD molecule together with interactions with a lipid that we tentatively identify as PIP₂. When comparing the effect of CBD on the TRPV1 and TRPV3 channels, which are also activated by CBD and 2-APB ([Hu et al., 2004](#)), we find that only TRPV3 channels are potently sensitized by CBD. Further, mutations at rTRPV1 sites that differ between TRPV1 and TRPV2 and that are located in the pore or the CBD binding region failed to confer strong sensitization by CBD. These findings establish that the robust sensitization by CBD observed in TRPV2 channels involves a CBD-specific allosteric mechanism that engages channel regions distant from the CBD binding site and the pore, and possibly ligand

interactions with multiple sites in the protein.

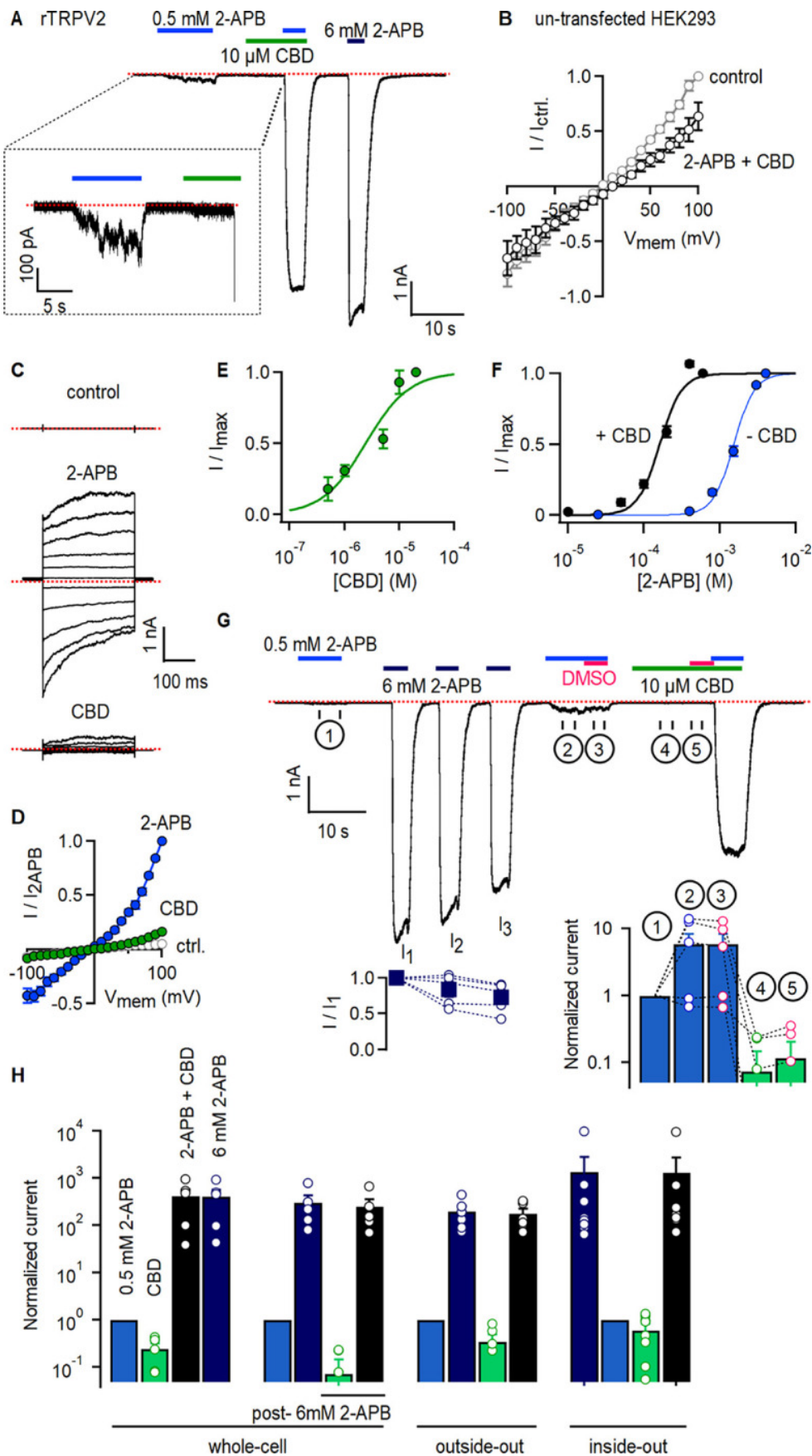
Results

CBD strongly sensitizes rTRPV2 channels to activation by 2-APB

We expressed rat TRPV2 (rTRPV2) channels in HEK293 cells and began by measuring the magnitude of the currents elicited by a low concentration of 2-APB (0.5mM) or a near-saturating concentration (10 μ M) of CBD ([Qin et al., 2008](#)) in the whole-cell configuration of the patch clamp at a holding potential of -80 mV. Even at this low concentration, 2-APB elicited currents that were much larger than those by CBD ([Figure 1A](#)). When 2-APB and CBD were applied together at the same concentrations, we observed large currents that were comparable to those measured in response to a concentration of 2-APB (6 mM) that maximally activates rTRPV2 channels ([Figure 1A](#)). Currents in the presence of 0.5 mM 2-APB were over two orders of magnitude larger in the presence of CBD than in its absence ([Figure 1H](#), first set of bar graphs). Importantly, 2-APB and CBD applied together elicited no increase in whole-cell currents from un-transfected cells recorded in response to voltage pulses from -100 to +100 mV ([Figure 1B](#)). In contrast, the same voltage-stimulation protocol elicited robust currents in rTRPV2-transfected cells when exposed to 0.5 mM 2-APB or 10 μ M CBD applied separately ([Figures 1C and 1D](#)). The sensitization caused by CBD is so strong that it becomes challenging to quantitate; at 0.5 mM 2-APB, channel activity is barely detectable in the whole-cell

configuration, and yet with CBD added currents reach

maximal activation levels ([Figure 1A](#) and [andH\).H](#)). The magnitude of sensitization we measured ([Figure 1H](#)) likely represents a lower bound for the sensitizing effect of CBD on rTRPV2 channels. We therefore analyzed data in a semi-quantitative manner without attempting to quantify the energetics associated with sensitization.



CBD strongly sensitizes rTRPV2 channels to activation by 2-APB in whole-cell and in excised patch

recordings.

(A) Representative whole-cell gap-free current recording at -80mV from a cell expressing rTRPV2 channels. The colored horizontal lines denote the duration of exposure to test compounds, and the red dotted line denotes the zero-current level. The insert shows a magnified view of a segment of the recording.

(B) Mean current-voltage relations recorded in control solution and in the presence of 0.5 mM 2-APB + $10\text{ }\mu\text{M}$ obtained from un-transfected cells in the whole-cell configuration ($n = 8$). **(C)** Representative current

families elicited by voltage steps from -100 to $+100\text{ mV}$ obtained from a rTRPV2-expressing cell exposed to control solution, 0.5 mM 2-APB or $10\text{ }\mu\text{M}$ CBD. The dotted lines indicate the zero-current level. **(D)** Mean current-voltage relations obtained from data as in (C) and normalized to the mean value at $+100\text{ mV}$ in the presence of 0.5 mM 2-APB. Data are shown as mean \pm SEM ($n = 5$).

(E) Dose-response relation for rTRPV2 channel activation by CBD measured at -80 mV in the whole-cell configuration (mean \pm SEM; $n = 4$). The continuous curve is a fit to the Hill equation with parameters: $\text{EC}_{50} = 4.3 \pm 1.4\text{ }\mu\text{M}$ and Hill coefficient (n_H) = 1.7 ± 0.1 .

(F) Concentration-response relations for rTRPV1 channel activation by 2-APB at -80 mV in the whole-cell configuration measured in the absence (blue symbols) or presence (black symbols) of $10\text{ }\mu\text{M}$ CBD (mean \pm SEM; $n = 7$). Hill equation parameters: no

CBD $\text{EC}_{50} = 15 \pm 0.05\text{ mM}$ Hill coefficient (n_H) = 2.2

± 0.2; 10 μM CBD, EC₅₀ = 159.9 ± 7.7 μM, Hill coefficient (n_H) = 2.9 ± 0.3. (G) Representative whole-cell gap-free recording at -80 mV in a rTRPV2-expressing cell. The bottom-left insert shows group data for the mean current amplitude at each of the three stimulations with 6 mM 2-APB, normalized to the amplitude at the first stimulation with 0.5 mM 2-APB (solid squares – mean ± SEM, n = 5; empty circles – data from individual cells). The bottom-right insert displays group data measured over the different intervals that indicated by circled numbers on the current trace, and normalized to the first stimulation with 0.5 mM 2-APB. The empty circles are data from individual cells. (H) Group data for experiments in the whole-cell configuration as in (A) - first set of bars (n = 5), (G) - second set of bars (n = 5), or from outside-out patches as in [Fig. 1 – Fig. Suppl. 3A](#) – third set of bars (n = 6) or inside-out patches as in [Fig. 1 – Fig. Suppl. 3B](#) – fourth set of bars (n = 9). Data was normalized to the first stimulation with 0.5 mM 2-APB and shown as mean ± SEM or values from individual cells (empty circles).

Figure 1 – source data 1. Excel file with group data from electrophysiological recordings shown in [Figure 1](#).

We were surprised at the minimal efficacy with which CBD activates rTRPV2 channels ([Figures 1A, CC and andD, D](#)), so we measured the magnitude of currents elicited by increasing concentrations of CBD in

rTRPV2-expressing cells. The resulting concentration-response relations ([Figure 1E](#)) confirm that CBD activates rTRPV2 channels with much higher affinity ($EC_{50} \sim 4 \mu M$) than 2-APB but also with much lower efficacy, and that rTRPV2 channels can be assumed to be fully bound by CBD at a concentration of $10 \mu M$ CBD. We next tested whether rTRPV2 channels display an increased apparent affinity for 2-APB when bound to CBD by measuring rTRPV2 channel activation at increasing concentrations of 2-APB in the presence and absence of $10 \mu M$ CBD, and found that the EC_{50} for 2-APB activation decreased ~ 10 -fold in the presence of CBD ([Figure 1F](#)).

The TRPV2 channel is reported to undergo sensitization upon stimulation with 2-APB that is irreversible over the duration of a patch-clamp experiment, leading to hysteresis in the 2-APB dose-response relations obtained pre- and post-sensitization: in most but not all patches, repeated short exposures to low concentrations of 2-APB were found to elicit progressively larger currents until reaching a plateau ~ 15 -fold larger than the initial response ([Liu and Qin, 2016](#)). Sensitization also reached saturation after a single short stimulation with a concentration of 2-APB that maximally activates channels ([Liu and Qin, 2016](#)). To investigate whether 2-APB and CBD sensitize rTRPV2 channels to a similar extent we performed experiments where we first briefly exposed cells to 0.5 mM 2-APB, then we stimulated

cells with a maximally activating concentration of 2-APB (6 mM), which we repeated three times to ensure all channels had become sensitized (I_1 , I_2 and I_3 , [Figure 1G](#)), and finally exposed cells to 0.5 mM 2-APB and 10 μ M CBD first applied separately and then together. We found that currents activated by 0.5 mM 2-APB increased nearly 10-fold after repeated stimulation with 6 mM 2-APB in some but not all cells ([Figure 1G](#), ① vs ②), whereas co-application with CBD increased currents by > 100-fold in all cells ([Figure 1G](#) and [and H, H](#), second set of bar graphs). The observed magnitude and cell-to-cell variability of 2-APB dependent sensitization is consistent with previously reported measurements ([Liu and Qin, 2016](#)), and markedly smaller than sensitization by CBD. These results indicate that the predominant states adopted by rTPRV2 channels when bound to CBD must be energetically different than those adopted by 2-APB-sensitized channels in the absence of ligands.

Recording solutions containing 2-APB and CBD also included dimethyl sulfoxide (DMSO) that we used to make stock solutions of both compounds, so the amount of DMSO applied to cells was larger in solutions that contained both agonists. To rule out an influence of DMSO on our results, in the same experiments described above we exposed cells to solutions with either 2-APB or CBD with added DMSO so that its concentration was the same as in solutions that contained both agonists together. We found that

~~the additional DMSO did not change the magnitude of~~

the currents in 0.5 mM 2-APB ([Figure 1G](#), ②vs ③) or 10 μ M CBD ([Figure 1G](#), ④ vs ⑤).

To rule out a direct chemical reaction between 2-APB and CBD, yielding a product with enhanced potency to activate the channel, we ran samples containing our recording solution (blank), 2-APB, CBD, and 2-APB and CBD mixed together, through a high-performance liquid chromatography (HPLC) system. We found that the elution time and height of the two peaks present in the sample with both agonists matched with the single peaks observed in the samples with either CBD or 2-APB, suggesting the two do not interact chemically ([Figure 1 – Fig. Supplement 1](#)).

In addition to being weakly sensitized by 2-APB, rTRPV2 channels are strongly and irreversibly sensitized by heat, in which channel activation with extreme heat resulted in a 10-fold decrease in the EC₅₀ for 2-APB ([Liu and Qin, 2016](#)). In addition, heat-sensitized rTRPV2 channels no longer require extreme temperatures (> 55 °C) to activate, showing current responses at temperatures at or below 40 °C ([Liu and Qin, 2016](#)). We therefore tested whether the mechanisms of rTRPV2 channel sensitization by CBD and heat are related. We reasoned that if this was the case, then the presence of CBD should facilitate channel activation by heat, and enable current responses at around 40 °C. Using rTRPV1 channel currents as a positive control for

+their high sensitivity to temperature changes in the

20–40 °C range, we successfully detected steeply temperature-dependent currents as previously described ([Figure 1 – Fig. Supplement 2A](#) and [E](#)) ([Caterina et al., 1997; Yao et al., 2010; Jara-Oseguera et al., 2016](#)).

When we performed experiments using cells expressing rTRPV2 channels we were unable to detect any temperature-dependent changes in current that were noticeably different from those measured under identical conditions in un-transfected cells ([Figure 1 – Fig. Supplement 2B, C](#) and [E](#)), as expected because the threshold for heat activation for rTRPV2 channels is > 55 °C ([Yao et al., 2011; Liu and Qin, 2016](#)). Interestingly, the responses in rTRPV2-expressing cells were the same in the absence and presence of CBD ([Figure 1 – Fig. Supplement 2D](#) and [E](#)), indicating that CBD does not strongly sensitize rTRPV2 channels to activation by heat. We also tested whether CBD sensitizes rTRPV2 channels to activation by the synthetic agonist probenecid ([Bang et al., 2007](#)), but we failed to detect any probenecid-elicited currents in the absence or presence of CBD (data not shown).

Finally, we tested if the sensitizing effect of CBD on activation of rTRPV2 channels by 2-APB also occurs in excised membrane patches devoid of many cellular components. Exposure of outside-out or inside-out patches expressing rTRPV2 channels to 0.5 mM 2-APB or 10 μM CBD alone elicited negligible currents ([Figure 1 – Fig. Supplement 3](#)), and similarly to our results in

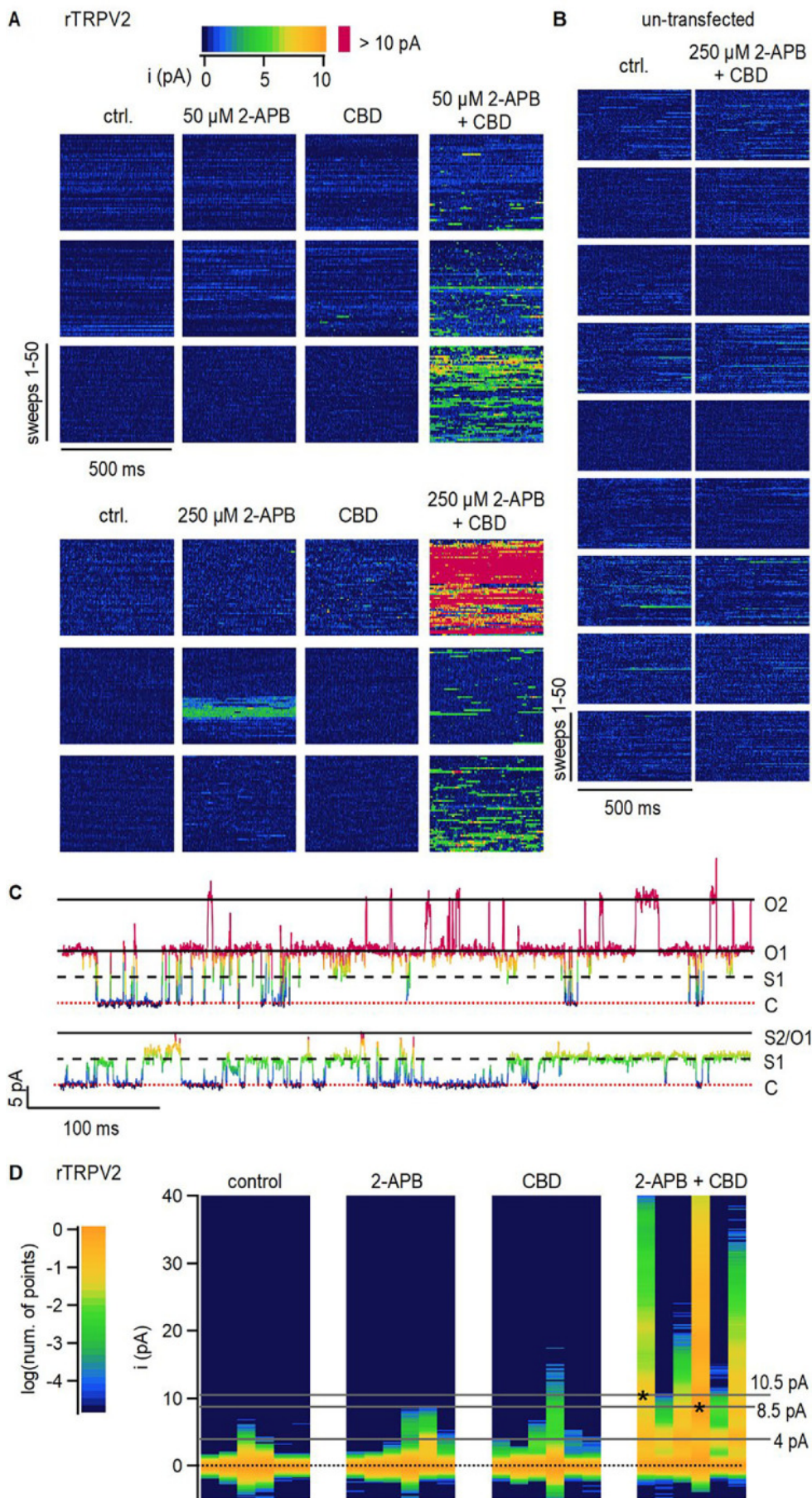
the whole-cell configuration, application of both

agonists together elicited very large currents of the same magnitude as those elicited in response to 6 mM 2-APB that maximally activates channels ([Figure 1H](#), third and fourth sets of bar graphs; [Figure 1 – Fig. Supplement 3](#)). These results indicate that patch excision does not disrupt sensitization of 2-APB responses by CBD, and that both agonists are capable of reaching their sites in the channel regardless of the side of the membrane to which they are applied.

rTRPV2 channel sensitization by CBD increases channel open probability

To determine whether CBD sensitizes rTRPV2 channels to activation by 2-APB by increasing channel open probability (P_o) we undertook single-channel recordings. Although we were unable to obtain patches containing a single channel because the rTRPV2 channel expresses extremely well in HEK293 cells, we obtained recordings from inside-out patches containing multiple channels under conditions where the P_o is very low and gating transitions of individual channels can be readily distinguished. For each patch we recorded channel activity in the absence of agonists (i.e. control), and in the presence of 2-APB and CBD applied separately or together. All recorded data are displayed in [Figure 2A](#) as two 3×4 arrays: each row in the array contains data from a different inside-out patch ($n = 6$), and columns separate data at different experimental conditions. For each element of the array, current sweeps are stacked along the vertical

axis (50 sweeps recorded at each experimental condition per patch) and the horizontal axis corresponds to the recoding duration of 500 ms per sweep. Individual data points are colored by current amplitude – see the color bar and the representative sweeps in [Figure 2C](#) for reference.



CBD sensitization of rTRPV2 channels involves an increase in open probability.

(A) Data obtained from six rTRPV2-expressing inside-out patches at +80 mV under conditions of low open probability. Each row shows data from a different patch, and columns separate between recordings at different experimental conditions. 50 current sweeps of 500 ms duration are displayed vertically stacked at each experimental condition for each patch. Data points at each sweep are colored by their current amplitude as indicated by the color-bar at the top. (B) Data obtained from nine inside-out patches at +80 mV obtained from un-transfected cells, displayed as in (A). (C) Representative current traces from the same rTRPV2-expressing patch in the presence of 50 μ M 2-APB and 10 μ M CBD showing two distinct open current amplitudes (S1 and O1) and simultaneous opening of two channels (O2). Data points in each trace are colored as in (A). The red dotted line indicates the zero-current amplitude measured when all channels are closed. (D) All-points histograms for data in (A). Each vertical lane is a histogram, with the single-channel current amplitude bins along the y-axis and the number of points per bin shown as a log-scale color heat-map (see scale bar on the left) and normalized to the peak centered at 0 pA (black dotted line). Histograms from each patch are displayed in the same order as in (A). Asterisks at peak values of 8.5 or 10.5 pA indicate the patches where these single-

channel amplitudes were observed.

With the exception of a high- P_o burst at 250 μM 2-APB observed in one patch, channel activity in the absence of agonists or in the presence of either of 2-APB or CBD applied separately was negligible, with most patches exhibiting no clearly identifiable opening events ([Figure 2A](#)). In contrast, exposure of patches to 2-APB and CBD together resulted in robust channel activity in all patches, with multiple simultaneous channel opening events observed in many of the patches ([Figure 2A](#) and [and C.C](#)). Exposure to 2-APB and CBD did not elicit changes in channel activity in patches from un-transfected cells ([Figure 2B](#)), strongly suggesting that the increases in channel activity observed in rTRPV2-expressing cells reflect a dramatic increase in P_o in rTRPV2 channels when CBD and 2-APB are simultaneously present.

To compare between data from different patches at each experimental condition, we generated all-points current amplitude histograms from each of our recordings shown in [Figure 2A](#); each vertical lane in [Figure 2D](#) is a histogram, with current-amplitude bins on the vertical axis and a color-scale to denote the logarithm of the normalized number of points per bin. For almost all patches, the histograms in control, 2-APB, or CBD have a single peak centered at 0 pA, the current amplitude when no channels are open. Consistent with a much greater P_o in the presence of 2-APB and CBD together, the corresponding

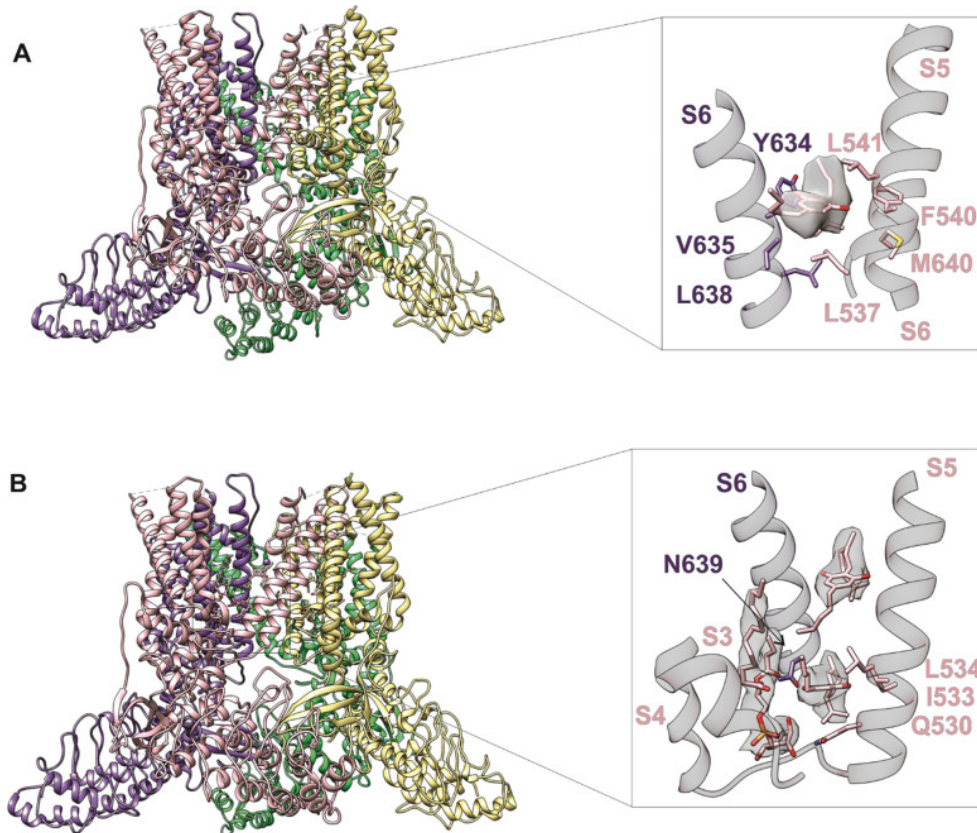
histograms all have robust peaks at larger amplitudes

representing the opening of one or more channels ([Figure 2D](#), right panel). We could not accurately determine single-channel current amplitudes in 2-APB or CBD because of the short duration and sparsity of openings when the agonists were applied separately. In the presence of 2-APB and CBD together the single-channel current amplitude was centered at around 4.3 pA in five out of the six patches, with one patch exhibiting a much larger open amplitude of 8.2 pA ([Figure 2D](#)). In one of the patches in the presence of the two agonists the open-channel current amplitude was initially ~4 pA but we also began observing openings with a larger current amplitude of 10.5 pA that became predominant for rest of the experiment ([Figure 2C](#) and [and D](#)). We are fairly confident that both amplitudes correspond to open rTRPV2 channels because we were able to observe multiple transitions between conductance levels when only one channel was open ([Figure 2C](#)). Together, these findings imply that rTRPV2 channels can undergo transitions between open states with different cation-conducting properties, as described for the closely related rTRPV1 channel ([Canul-Sánchez et al., 2018; Geron et al., 2018](#)) and the RTx-sensitive TRPV2-QM variant ([Zhang et al., 2016](#)), and firmly establish that the CBD-dependent sensitization of rTRPV2 channels arises from increased open probability of channels bound to CBD and 2-APB.

Interaction sites for CBD in the rTRPV2 channel.

To further explore the mechanism by which CBD sensitizes rTRPV2 to activation by 2-APB, we set out to confirm where CBD binds ([Pumroy et al., 2019, 2022](#)) and to solve structures of rTRPV2 with both ligands bound. We expressed an mVenus-tagged construct of full-length rTRPV2 in mammalian cells, purified and reconstituted the protein into lipid nanodiscs using MSP1E3D1 ([Matthies et al., 2018](#)), and solved its structure using cryo-EM in the presence of both CBD and 2-APB ([Figure 3 – Fig. Supplement 1–4, Table 1](#)). In our initial classification and refinement, we determined the structure of rTRPV2 spanning residues F75 to S728, including the transmembrane (TM) regions along with portions of the N- and C-termini and observed well-defined density for CBD between the S5 and S6 helices ([Figure 3A](#)), which we termed conformation A. The overall structure of rTRPV2 in conformation A and the location where CBD binds are remarkably similar to a previously published structure of rTPRV2 with CBD bound ([Pumroy et al., 2019](#)), as well as a more recent structure obtained in the presence of CBD and 2-APB ([Pumroy et al., 2022](#)) – in each of these instances the internal pore remains closed and the structures are likely to represent a desensitized state. Although the overall resolution of conformation A was 3.26 Å, we could not see any density corresponding to 2-APB, including regions where 2-APB has been reported to bind to either TRPV2 or TRPV3 ([Figure 3 – Fig.](#)

Supplement 5A) ([Singh et al., 2018b, 2018a; Zubcevic et al., 2019; Pumroy et al., 2022; Su et al., 2023](#)).



Identifying CBD binding sites in TRPV2.

(A) Overall structure of the rTRPV2 channel in lipid nanodiscs in conformation A with one CBD molecule bound to each monomer (pdb ID 8FX8). Magnified view of the single CBD binding site was shown in the right panel. Both CBD and interacting residues are presented in stick with the cryo-EM density (EMD-29526) corresponding to CBD shown as a white surface. (B) Overall structure of the rTRPV2 channel in lipid nanodiscs in conformation B with two CBD molecules bound to each monomer (pdb ID 8FXG). Magnified view of the two CBD binding sites are shown

in the right panel. CBD with interacting residues and

lipid were presented in stick and cryo-EM density (EMD-29532) corresponding to CBD and lipid are shown as a white surface.

Table 1.

Cryo-EM data collection, refinement and validation statistics

	Conformation A	Conformation B
Data collection and processing		
Magnification	105,000	105,000
Voltage (kV)	300	300
Electron exposure (e ⁻ /Å ²)	52	52
Defocus range (μm)	−0.5 to −1.5	−0.5 to −1.5
Pixel size (Å)	0.43	0.43
Symmetry imposed	C4	C4
Initial particle images (no.)	1,665,271	1,665,271
Final particle images (no.)	322,102	43,071
Map resolution (Å)	3.26	3.44
FSC threshold	0.143	0.143
Refinement		
Initial model used (PDB code)	6U84	6U84
Model resolution (Å)	3.49	3.75
FSC threshold	0.5	0.5
Map sharpening B-factor (Å ²)	−55	−50
Model composition		
Non-hydrogen atoms	18077	18481
Protein residues	2388	2384
Ligands	9	17
R.m.s deviations		
Bond lengths (Å)	0.004	0.003
Bond angles (°)	0.934	0.606
B factor(Å²)		
Protein	108.32	71.52
Ligand	117.89	61.93
Validation		
MolProbity score	1.47	1.32

Clashscore	4.61	3.26
Conformation A Conformation B		
Poor rotamers (%)	0	0.46
Ramachandran Plot		
Favored (%)	96.47	96.76
Allowed (%)	3.53	3.24
Disallowed (%)	0	0

To identify where 2-APB binds in the presence of CBD, we undertook further focused classification of the TM region without image alignment, and subsequent refinement yielded a second conformation at 3.44 Å, which we refer to as conformation B ([Figure 3B](#); [Figure 3 – Fig. Supplement 1–4, Table 1](#)). In this new conformation, we observed density for two CBD molecules per subunit, one positioned similarly to conformation A and a second located nearby the S5 and S6 helices and the S4-S5 linker towards the intracellular side of the protein ([Figure 3B](#)). We also observe a well-defined density at the vanilloid site of a lipid molecule interacting with and likely stabilizing the second CBD molecule at this new site ([Figure 3B](#)). Because the headgroup density for this lipid is relatively large, we tentatively assigned the lipid as phosphatidylinositol. In conformation A and earlier structures of TRPV2, the S4-S5 linker adopts a helical secondary structure, whereas in conformation B, residues at the C-terminal end of the S4-S5 linker are incorporated into the S5 helix to lengthen that TM, and the remaining residues in the linker adopt an extended loop ([Figure 3B](#)). Importantly, the position of the vanilloid lipid in conformation B resembles density

attributed to lipid in rTRPV2 structures obtained in the

presence of 2-APB together with CBD that were proposed to represent an activated state of the channel ([Pumroy et al., 2022](#)). In both of these instances, the position of the lipid is closer to the S4-S5 linker when compared to vanilloid lipid observed in other structures of TRPV2 or TRPV1 ([Figure 3 – Fig. Supplement 6](#)) ([Zhang et al., 2021; Su et al., 2023](#)). However, as with conformation A, we see no clear density for 2-APB in conformation B, including those regions where 2-APB has been reported to bind to either TRPV2 or TRPV3 ([Figure 3 – Fig. Supplement 5B](#)). From these results we conclude that it remains unclear where 2-APB binds to rTRPV2 in the presence of CBD, but that CBD can bind to two sites within each subunit of rTRPV2 to modulate its activity, with binding to the most intracellular site involving stabilizing interactions with the lipid at the vanilloid site and a localized conformational change in the S4-S5 linker.

We note that a much larger number of particles were used to refine conformation A (322,102) compared to conformation B (43,071) ([Figure 3 – Fig. Supplement 2](#)), suggesting that the binding of CBD to the more extracellular site has higher occupancy compared to the more intracellular site. This difference in CBD occupancy might suggest that the affinity of CBD is higher for the more extracellular site, at least in the state favored by the biochemical conditions used for structural determination. Another possibility is that the

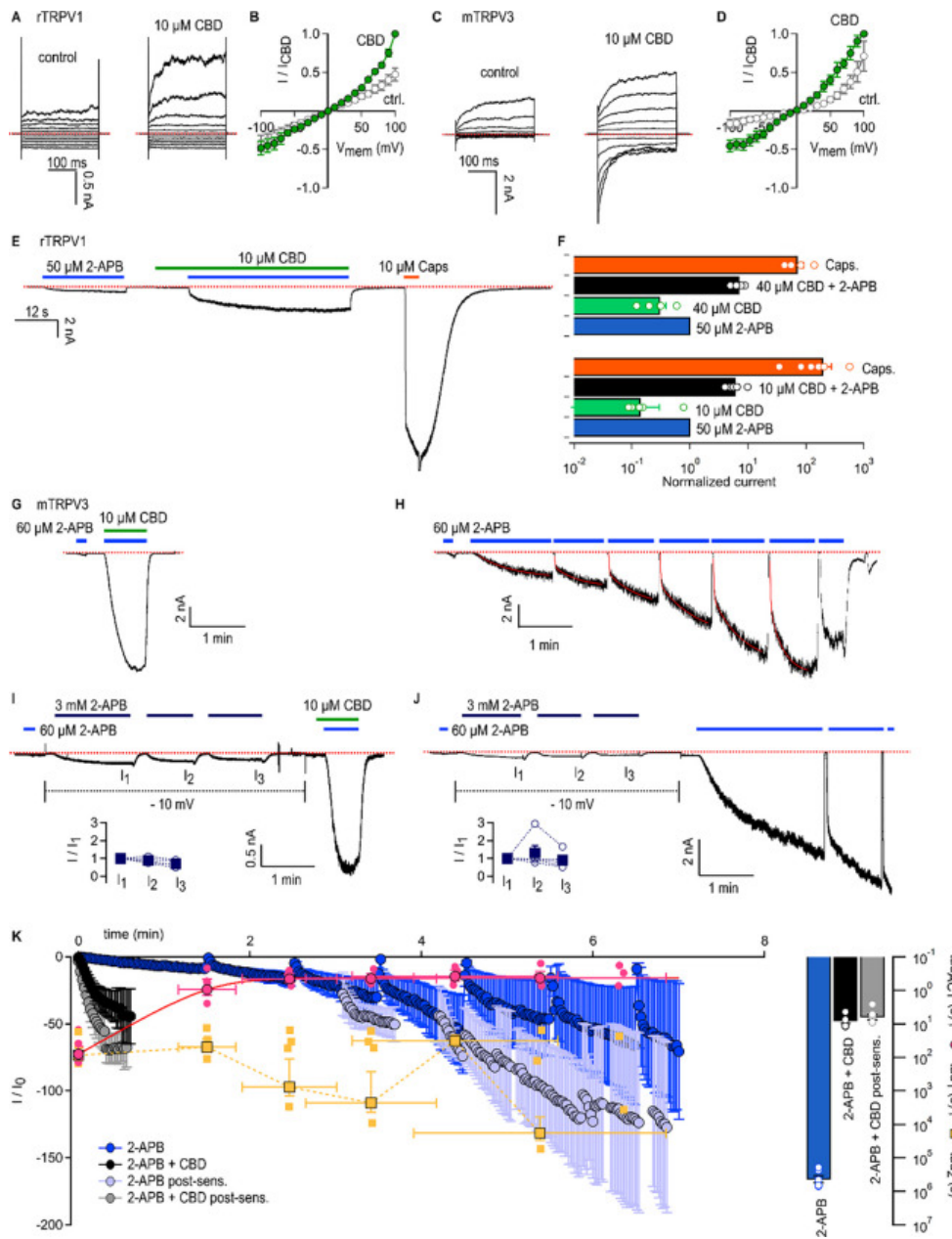
second site for CBD identifies an access pathway for

CBD to enter the TM domain from the intracellular side of the membrane and that the conformational change of the S4-S5 linker that lengthens S5 opens this access pathway. Finally, it is possible that conformation B is only transiently populated during activation or desensitization of rTRPV2. The conformational change in the S4-S5 linker observed in conformation B is interesting because this structural element plays a critical role in coupling conformational changes in the S1-S4 domain to the pore domain where the gate resides.

CBD sensitizes rTRPV1 channels weakly and mTRPV3 channels strongly to activation by 2-APB.

Rat TRPV1 (rTRPV1) and mouse TRPV3 (mTRPV3) channels share 49 and 42% amino acid sequence identity with rTRPV2, respectively, and accumulating evidence suggests that some agonists follow similar mechanisms to activate these three channels ([Yang et al., 2016](#); [Zhang et al., 2016, 2019](#); [Zubcevic et al., 2018](#); [Jara-Oseguera et al., 2019](#); [Deng et al., 2020](#); [Shimada et al., 2020](#)). In addition, the three channels can be activated by 2-APB ([Hu et al., 2004](#)), and previous reports used Ca^{2+} -imaging to show that CBD can also stimulate TRPV1 ([Bisogno et al., 2001](#); [Ligresti et al., 2006](#); [De Petrocellis et al., 2012](#); [Iannotti et al., 2014](#)) and TRPV3 ([De Petrocellis et al., 2012](#)) channels with low micromolar affinity. We therefore tested whether CBD exerts a similar sensitizing effect on rTRPV1 and mTRPV3 channels.

First, we confirmed that 10 μ M CBD can elicit currents in rTRPV1 or mTRPV3-expressing cells by recording current-voltage relations in the absence and presence of CBD and found that for both channels 10 μ M CBD noticeably increased currents relative to control (Figure 4A–D).



CBD sensitizes rTRPV1 channels weakly and mTRPV3 channels strongly to activation by 2-APB.

(A) Representative whole-cell current families obtained

from rTRPV1 expressing cells in control or in the presence of 10 μ M CBD. Currents were elicited by voltage steps from -100 to +100 mV. The red dotted line denotes the zero-current level. (B) Steady-state current-voltage relations obtained from data as in (A) and normalized to the steady-state current magnitude at +100 mV in CBD. Data is shown as mean \pm SEM ($n = 6$). (C) Representative whole-cell current families from mTRPV3 expressing cells obtained as in (A). (D) Steady-state mTRPV3 channel current-voltage relations obtained from data as in (C) (mean \pm SEM, $n = 7$). (E) Representative whole-cell recording at -80 mV obtained from a rTRPV1-expressing cell. (F) Group data from experiments as in (E) obtained using 10 or 40 μ M CBD and normalized to the current magnitude measured at steady state during the first stimulation with 50 μ M 2-APB. Data are shown as mean \pm SEM (10 μ M CBD, $n = 6$; 40 μ M CBD, $n = 5$) or as individual cells (empty circles). (G) Representative whole-cell gap-free recording at -60 mV obtained from a cell expressing mTRPV3 channels stimulated with 2-APB and CBD. The first exposure to 2-APB alone (10 s duration) was used for normalization. (H) Representative experiment showing repeated stimulation with 2-APB. The first exposure to 2-APB (10 s duration) was used for normalization. Red curves are fits to a double-exponential function of time, with time-constants shown on (K) in magenta and yellow as mean \pm SEM (filled symbols) or individual fit values (open symbols). (I, J) Representative experiments for sensitized responses to (I) 2-APB and CBD or (J) 2-

APB alone measured after three exposures to 3 mM 2-APB applied at -10 mV to preserve patch integrity (dotted black lines). The first exposure to 2-APB (10 s duration) was used for normalization. The insert shows current amplitudes at each stimulation with 3 mM 2-APB (filled squares, mean \pm SEM; empty circles, data from individual cells, $n = 5$). (K) Mean time-courses for mTRPV3 channel activation by 60 μ M 2-APB in the absence (blue symbols) or presence of 10 μ M CBD (black symbols), measured in experiments as in (G) and (H), as well as sensitized responses to 2-APB (light blue symbols) or 2-APB + CBD (grey symbols) measured as in (I) and (J). The time-course for the sensitized response to 2-APB alone does not start at $t = 0$ to account for the sensitizing exposures to 3 mM 2-APB. Data are shown as mean \pm SEM ($n = 5$ for each condition). Data were fit to a mono-exponential function of time, with time constants shown as mean \pm SEM (bars) or individual data points. The magenta curve is a fit to a mono-exponential function.

Figure 4 – source data 1. Excel file with group data from electrophysiological recordings shown in [Figure 4B](#) and [andDD](#).

Figure 4 – source data 2. Excel file with group data from electrophysiological recordings shown in [Figure 4F](#).

Figure 4 – source data 3. Excel file with group data from electrophysiological recordings shown in [Figure](#)

4I-K.

We next probed for CBD-dependent sensitization in cells expressing rTRPV1 channels. We performed experiments where we exposed cells to 50 μ M 2-APB and 10 μ M CBD, first applied separately and then together, and finally we applied 10 μ M capsaicin to maximally activate channels. To our surprise, we observed only moderate sensitization of the response to 2-APB in the presence of CBD vs its absence (< 10-fold increase), and sensitized currents were much smaller than the maximal currents recorded in the presence of capsaicin ([Figure 4E](#) and [and F](#)). In experiments using a higher concentration of CBD (40 μ M) we obtained similar results, indicating that 10 μ M CBD is enough to bind most rTRPV1 channels in the membrane, and that CBD-bound rTRPV1 are not strongly sensitized to activation by 2-APB, contrary to our observations with rTRPV2 channels.

We then tested the sensitizing effect of CBD on mTRPV3-expressing cells. We used a concentration of 2-APB that maximally activates channels (60 μ M), albeit with extremely slow kinetics due to the large energy barrier associated with the activation of this channel ([Liu et al., 2011](#)). Following activation, the energy barrier in the reverse direction (i.e. away from the activated state) is even larger, resulting in the irreversible sensitization of channels whereby the kinetics of activation by 2-APB become much faster

([Liu et al., 2011](#); [Zubcevic et al., 2019](#)). We found that a brief 10-second exposure to 2-APB resulted in a slow and minimal increase in current, whereas exposing the same cell to 2-APB together with CBD resulted in maximal current activation with a time constant < 10 seconds ([Figure 4G](#) and [andK\).K](#)). In contrast, in experiments where cells were repeatedly exposed to 60 μ M 2-APB in the absence of CBD, currents took several minutes to reach maximal activation ([Figure 4H](#) and [andK\),K](#)), consistent with previous observations ([Liu et al., 2011](#); [Zubcevic et al., 2019](#); [Deng et al., 2020](#)). After the first and second stimulation with the agonist, currents elicited by 2-APB increased bi-exponentially ([Figure 4H](#) and [andK\),K](#), pink and yellow symbols), likely reflecting the fractions of sensitized (fast activation) and non-sensitized (slow activation) channels in the cell membrane. Notably, the time constant for the fast kinetic component is similar to that for activation in the presence of 2-APB and CBD together ([Figure 4K](#)), suggesting that CBD binding strongly sensitizes mTRPV3 channels by lowering the energy barrier for activation by 2-APB.

Our results so far indicate that CBD is more efficient at sensitizing mTRPV3 channels than 2-APB at 60 μ M. We next tested whether 2-APB at a much higher concentration (3 mM) would sensitize channels much more rapidly. We first found that pre-stimulation of cells with 3 mM 2-APB had negligible effect on the

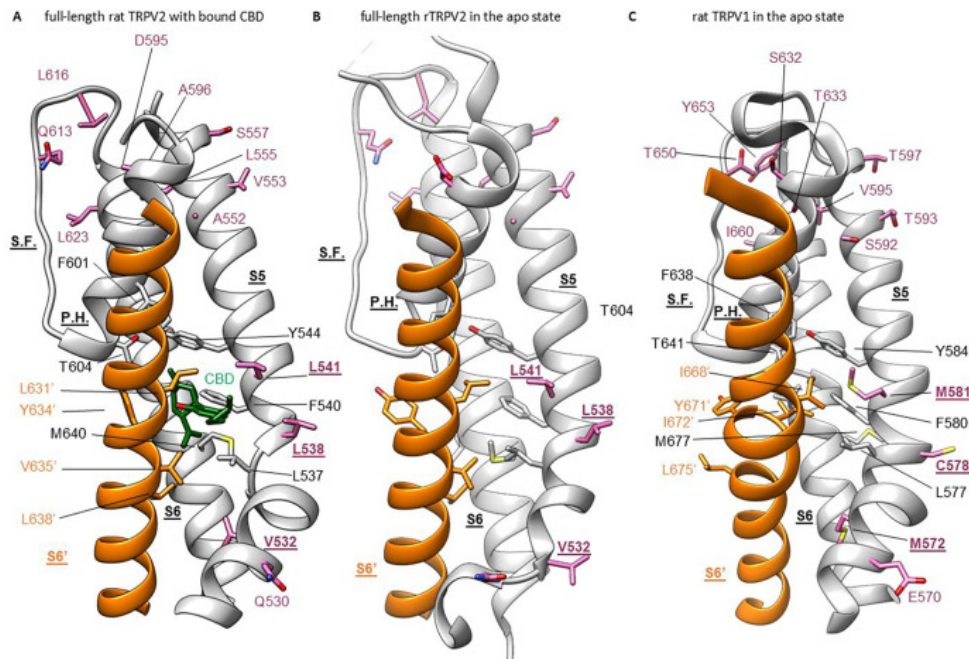
kinetics of activation by 60 μ M applied together with

CBD, confirming that these conditions maximally sensitize all channels in the recorded cell membrane ([Figure 4I](#) and [andK\).K](#)). In contrast, we found that currents elicited by 60 μ M 2-APB remained bi-exponential and continued to slowly increase after pre-stimulation with 3 mM 2-APB for > 1.5 minutes ([Figure 4J](#) and [andK\).K](#)). These results establish that CBD is a much weaker mTRPV3 channel agonist than 2-APB, but has a more potent sensitizing effect, similarly to our results with rTRPV2 channels. The absence of a strong sensitizing effect of CBD in rTRPV1 channels points to a key energetic difference regarding activation of rTRPV1 channels by 2-APB relative to rTRPV2 and mTRPV3 channels.

Structural determinants of sensitization by CBD in rTRPV2 and rTRPV1 channels

We next sought to identify the structural determinants for the strong sensitization by CBD observed in the rTRPV2 channel. The CBD site first identified in the full-length rTRPV2 channel ([Pumroy et al., 2019](#)) shows high conservation at the amino acid sequence level between the TRPV1, TRPV2 and TRPV3 channels ([Figure 5](#) and [Figure 5 – Fig. Supplement 1](#)). Under the assumption that sensitization in CBD-bound rTRPV2 and mTRPV3 channels follows a similar mechanism, we began by inspecting the amino acid sequence alignment between the three channels, and identified three residues in the pore S5 helix and the S4-S5 linker that are identical in rTRPV2 and mTRPV3

channels and different in rTRPV1 channels, and are also located very close to the CBD site observed previously and confirmed by us ([Figure 5](#) and [Figure 5 – Fig. Supplement 1](#)). We generated six mutant channels where we individually swapped each of the non-conserved residues between the rTRPV2 (V532M, L538C, L541M) and rTRPV1 channels (M572V, C578L, M581L). For each channel we also generated a double (rTRPV2 L538C+L541M; rTRPV1-C578L+M581L) and a triple mutant (rTRPV2-V532M+L538C+L541M; rTRPV1-M572M+C578L+M581L). Our hypothesis was that if those amino acid side-chain differences determine the strong or weak sensitization to 2-APB in CBD-bound rTRPV2 or rTRPV1 channels, respectively, then these introduced mutations should weaken sensitization in rTRPV2 channels and strengthen it in rTRPV1 channels.

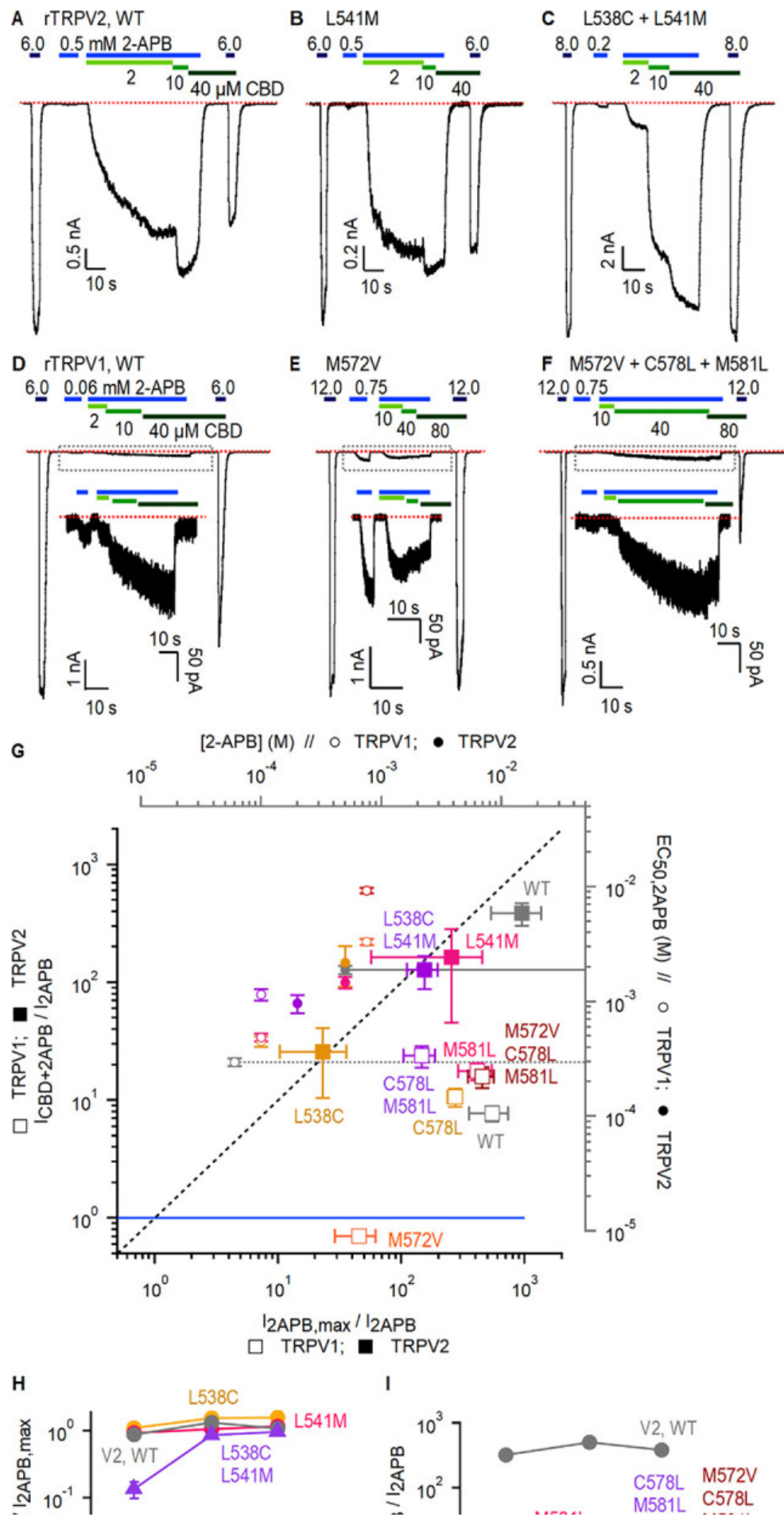


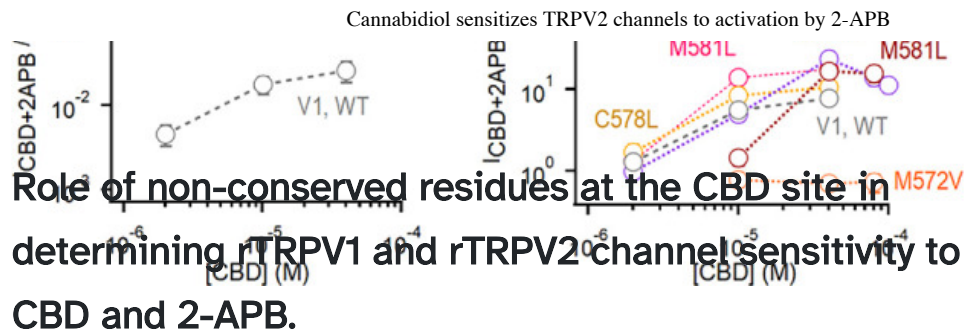
CBD binding site in TRPV2 channels and its conservation in TRPV1 channels.

(A) Structure of full-length rTRPV2 in nanodiscs with CBD bound in conformation A (with one CBD per subunit; pdb ID 8FX8). The S6 helix from one subunit is shown in orange, and in the adjacent subunit the S5 and S6 helices, the selectivity filter (S.F.), the pore-helix (P.H.), and the S4-S5 linker helix are shown in grey. Residues near the CBD site are shown in stick representation, and the bound CBD molecule in green. Residues that are similar in rTRPV2 and mTRPV3 channels but different in rTRPV1 channels are shown in purple. **(B)** Structure of apo full-length rTRPV2 in nanodiscs (pdb ID 6U84) ([Pumroy et al., 2019](#)). Same color coding as in A. **(C)** Structure of apo rTRPV1 (pdb ID 5IRZ) ([Gao et al., 2016b](#)) depicting the CBD binding region from rTRPV2. Same color coding as in A and B.

For each channel variant we measured the concentration-response relation for 2-APB ([Figure 6 – Fig. Supplement 1E](#) and [H](#)), and used for experiments concentrations of 2-APB that maximize the dynamic range between CBD-sensitized and non-sensitized responses to 2-APB; these concentrations used in experiments are plotted against the EC₅₀ for 2-APB in [Figure 6G](#) (filled and empty circles). To test our hypothesis we performed experiments where (1) we first established the maximal current elicited by 2-APB (I_{2APB,max}). We then (2) measured currents at a much lower concentration of 2-APB (I_{2APB}, later used for normalization), first alone and then (3–5) applied

together with increasing concentrations of CBD ($I_{CBD+2APB}$). Next, we (6) removed 2-APB still in the presence of CBD to assess activation by CBD alone, and finally (7) we maximally activated channels with 2-APB ($I_{2APB,max}$) to estimate to extent of channel desensitization during the experiment ([Figure 6A–F](#) and [Figure 6 – Fig. Supplement 1 A–D, E–G](#)). To visualize results, we plotted the fold-increase in current caused by CBD-dependent sensitization ($I_{CBD+2APB}/I_{2APB}$) relative to the fold-increase in current caused by a maximally activating concentration of 2-APB ($I_{2APB,max}/I_{2APB}$) ([Figure 6G](#), filled and empty squares) – the larger the vertical separation of the data from the dotted diagonal, the weaker the sensitization by CBD.





(A-C) Representative gap-free whole-cell recordings at -80 mV obtained from cells expressing WT or mutant rTRPV2 channels. Horizontal bars denote the time of exposure to 2-APB (blue bars, mM concentrations) or CBD (green bars, μ M concentrations). The red dotted line denotes the zero-current level. **(D-F)**

Representative gap-free whole-cell recordings at -80 mV obtained from cells expressing WT or mutant rTRPV1 channels. The inserts show magnified views of the current traces boxed by the dotted black lines. **(G, squares)** Group data for WT and mutant rTRPV1 (empty symbols) and rTRPV2 (filled symbols) channels obtained from experiments as in (A-F) showing the relation between the normalized sensitized response to 2-APB ($I_{CBD+2APB}/I_{2APB}$, left axis) and the maximal response to 2-APB ($I_{2APB,max}/I_{2APB}$, bottom axis). The blue line denotes $I_{CBD+2APB}/I_{2APB} = 1$ where the response to 2-APB in the presence of CBD is the same as in its absence (i.e. no sensitization). Data are shown as mean \pm SEM (WT rTRPV2, $n = 4$; L538C, $n = 4$; L541M, $n = 4$; L538C+L541M, $n = 4$; WT rTRPV1, $n = 5$; M572V, $n = 5$; C578L, $n = 5$; M581L, $n = 5$; C578L+M581L, $n = 5$; M572V+C578L+M581L, $n = 6$).

(G, circles) Relation between the EC_{50} for channel

activation by 2-APB (right axis) and the concentration

of 2-APB used in experiments as in (A-F) to probe sensitization by CBD (top axis) in WT and mutant rTRPV1 (empty symbols) and rTRPV2 (filled symbols) channels. The EC₅₀ values for WT rTRPV1 and rTRPV2 channels are highlighted by grey dotted and solid lines, respectively. EC₅₀ data obtained from fits to the Hill equation and shown as mean ± SEM (WT rTRPV2, n = 5; L538C, n = 4; L541M, n = 4; L538C+L541M, n = 3; WT rTRPV1, n = 5; M572V, n = 5; C578L, n = 5; M581L, n = 5; C578L+M581L, n = 4; M572V+C578L+M581L, n = 4; dose-response relations shown in [Fig. 6 – Fig. Suppl. 1E](#) and [H](#)). (H) Mean sensitized response of WT and rTRPV2 channel mutants to 2-APB ($I_{CBD+2APB}$) relative to the maximal activation by 2-APB ($I_{2APB,max}$) as a function of the concentration of CBD that was used to sensitize channels, obtained from experiments as in (A-C). Data for WT rTRPV1 is also shown as reference. (I) Mean sensitized response to 2-APB ($I_{CBD+2APB}$) relative to the non-sensitized response (I_{2APB}) shown as a function of the concentration of CBD that was used to sensitize channels, obtained from experiments as in (D-F).

Figure 6 – source data 1. Excel file with group data from electrophysiological recordings of CBD-dependent sensitization shown in Figure 6G-H, obtained from experiments as in (A)-(F). These data are also displayed on [Figure 6 – Supplement 1F-G](#).

Figure 6 – source data 2. Excel file with 2-APB dose-response relation data for rTRPV1 and rTRPV2 mutants shown in Figure 6G. These data are also displayed in [Figure 6 – Fig. Supplement 1E, H and I](#).

Mutations at position V532 or M572 in the S4-S5 linker had the largest impact on function in both channels: cells expressing rTRPV2 channels carrying the V532M mutation didn't respond to 2-APB or CBD (data not shown), whereas the rTRPV1-M572V mutant completely lacked sensitization by CBD ([Figure 6E](#), [,G,G](#), and [andII](#) and [Figure 6 – Fig. Supplement 1G](#)). Notably, the triple rTRPV1 mutant M572M+C578L+M581L had restored sensitization by CBD similar to WT rTRPV1 channels, although higher concentrations of CBD were required for maximal sensitization ([Figure 6 F](#), [,G,G](#), and [andI;I](#); [Fig. 6 – Fig. Supplement 1G](#)). rTRPV1 channels carrying the M572V mutation also had a severely reduced sensitivity to 2-APB; the EC₅₀ for 2-APB in the single mutant was ~10-fold larger than WT, and channels containing the triple mutation failed to maximally activate at concentrations up to 15 mM 2-APB ([Figure 6G](#) and [Figure 6 – Fig. Supplement 1H](#)). In stark contrast, the M572V mutation had a limited effect on capsaicin sensitivity of rTRPV1 channels: the EC₅₀ for capsaicin increased by less than 5-fold in both single and triple mutants ([Figure 6 – Fig. Supplement 1I](#)).

rTRPV1 channel mutations C578L and M581L in the S5

helix restored sensitivity to CBD in the M572V background, but otherwise when introduced as single or double mutations without M572C they had only moderate effects on sensitivity to 2-APB and no apparent effect on sensitization by CBD or activation by capsaicin ([Figure 6 G](#) and [and I; I](#); [Figure 6 – Fig. Supplement 1B–D, G–I](#)). The single mutations L538C and L541M had minimal impact on rTRPV2 channel function, and the double mutant L538C + L541M displayed only a mildly decreased sensitivity to CBD relative to WT ([Figure 6 B, C, C, GG](#) and [and H; H](#); [Figure 6 – Fig. Supplement 1A, E](#) and [E](#)). Interestingly, this mutant exhibited a somewhat decreased EC₅₀ for 2-APB ([Figure 6G](#) and [Figure 6 – Fig. Supplement 1E](#)).

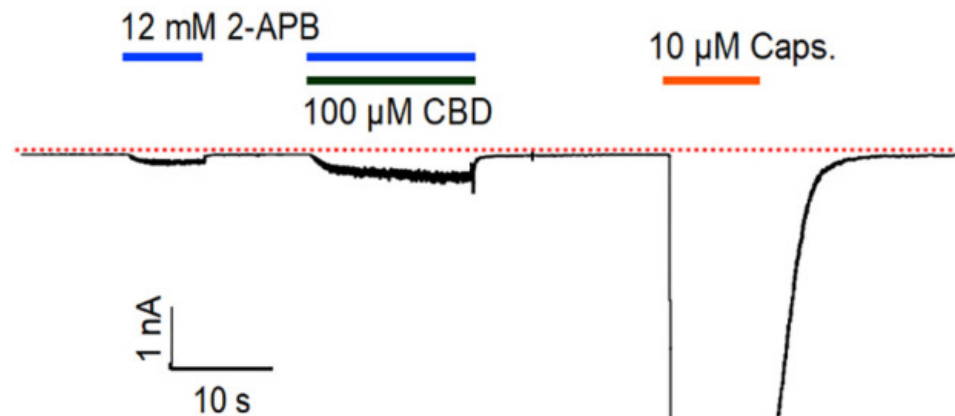
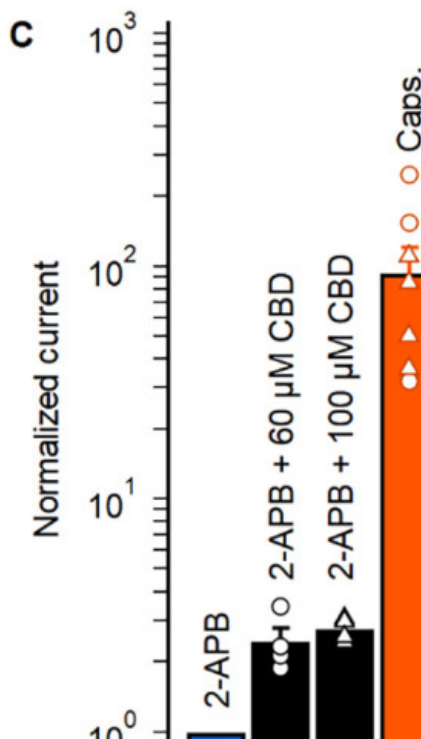
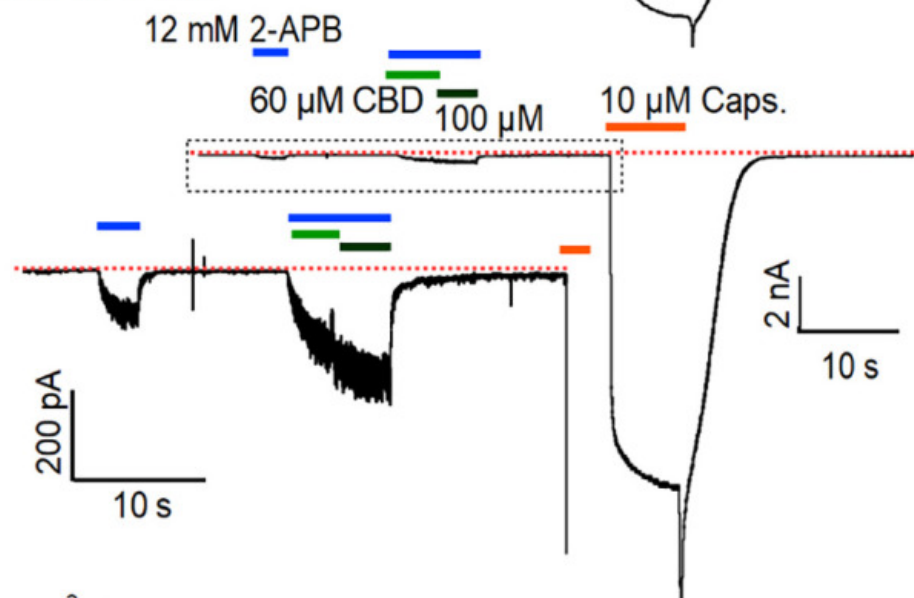
Our results thus far show that substitutions at non-conserved positions close to the CBD site can influence sensitivity of both rTRPV2 and rTRPV1 channels to 2-APB and CBD, without strongly influencing capsaicin sensitivity in rTRPV1 channels; notably, even the rTRPV1 mutation that caused a very strong reduction in 2-APB and CBD sensitivity, M572V, had only a minimal influence on activation by capsaicin. Together, these results highlight the importance of the S5 helix and the proximal S4-S5 linker region for activation of rTRPV2 and TRPV1 channels by 2-APB, and are also consistent with the proposed binding site for CBD in rTRPV2 channels ([Pumroy et al., 2019](#)), suggesting the site could be conserved in rTRPV1 channels. However, the structural determinants for the difference in the magnitude of the

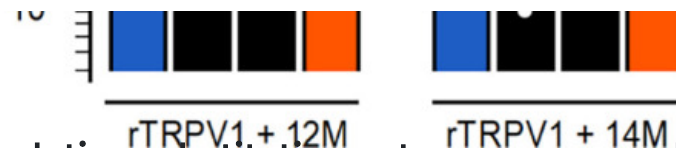
Determinants for the difference in the magnitude of the

sensitization by CBD in rTRPV2 and rTRPV1 channels must lie somewhere else.

We and others have shown that residues in the pore-domain can dramatically tune sensitivity to activators in TRPV1-3 channels ([Jordt et al., 2000](#); [Grandl et al., 2008, 2010](#); [Jara-Osegueda et al., 2016](#); [Zhang et al., 2019](#)), so we proceeded to interrogate a possible role of amino acid sequence differences between the pore domains of rTRPV2 and rTRPV1 channels. We found 8 additional positions in the pore domain that are conserved in rTRPV2 and mTRPV3 channels but not in rTRPV1 channels ([Figure 5](#) and [Figure 5 – Fig. Supplement 1](#)) – A552, V553, L555 and S557 in the S5 helix of rTRPV2 (S592, T593, V595, T597 in rTRPV1), D595 and A596 in the pore helix of rTRPV2 (S632, T633), Q613 above the selectivity filter in rTRPV2 (T650 in rTRPV1), and L623 in the S6 helix of rTRPV2 (I660 in rTRPV1). We cumulatively substituted each of these positions in rTRPV1 with the amino acids present in rTRPV2, together with four substitutions near the CBD site (E570Q, M572V, C578L, M581L in TRPV1), and tested whether CBD had a stronger sensitizing effect in the resulting rTRPV1-12M channel. The sensitivity to 2-APB was highly disrupted in rTRPV2-12M channels ([Figure 7A](#)), with a concentration of 12 mM 2-APB producing a similar extent of activation relative to 10 µM capsaicin as a concentration of 50 µM 2-APB in WT rTRPV1 channels. ([Figure 4E](#) and [andF](#)). In contrast to the ~~heavily impaired sensitivity to 2-APB, sensitivity to~~

CBD, and the magnitude of the sensitization caused by CBD appeared to be minimally affected ([Figure 7A](#) and [and C.C](#)). Capsaicin sensitivity was also seemingly less affected, as we observed robust responses to a concentration of 10 μ M that were much greater than those elicited by the highest concentration of 2-APB that we tested. Finally, we introduced two additional substitutions at the extracellular S6 loop (Y653L and D654R) of rTRPV1-12M channels, which are not conserved between rTRPV2, mTRPV3, and TRPV1 channels ([Figure 5 – Fig. Supplement 1](#)), and found that the resulting channels, rTRPV1-14M, behave very similarly to rTRPV1-12M channels ([Figure 7B](#) and [and C.C](#)). Together, our results suggest that multiple sites in the protein, including sites distant from the pore domain and CBD-binding sites, contribute to determining the magnitude of sensitization caused by CBD in rTRPV2 and rTRPV1 channels. Our results also show that for rTRPV1, activation by 2-APB is much more sensitive to perturbations in the pore domain and potential CBD-site than sensitivity to CBD and capsaicin.

A rTRPV1 + 12M**B rTRPV1 + 14M**



Cumulative substitutions at non-conserved positions in the rTRPV1 pore do not enhance sensitization.

Representative time courses for (A) rTRPV1-12M channels (E570Q + M572V + C578L + M581L + S592A + T593V + V595L + T597S + S632D + T633A + T650Q + I660L) or (B) rTRPV1-14M channty54rels (E570Q + M572V + C578L + M581L + S592A + T593V + V595L + T597S + S632D + T633A + Y653L + D654R + T650Q + I660L) displaying sensitization by CBD of the response to 12 mM 2-APB. The red dotted line indicates the zero-current level. The insert in (B) is a magnification of the region within the dotted box. Concentrations of 60 or 100 µM CBD were tested in separate experiments for rTRPV1-12M and in the same experiment for rTRPV1-14M. (C) Group data for the experiments in (A) and (B), showing leak-subtracted current responses to each of the stimuli, normalized to the current magnitude in the presence of 12 mM 2-APB. Data points from individual experiments are shown as open symbols. The triangles are not normalized capsaicin response in the experiments for rTRPV1-12M and 100 µM CBD. Data are shown as mean ± SEM ($n = 4$ for rTRPV1-12M and 60 or 100 µM CBD; $n = 5$ for rTRPV1-14M).

Figure 7 – source data 1. Excel file with group data from electrophysiological recordings of CBD-dependent sensitization shown in [Figure 7](#).

Discussion

The goal of the present study was to characterize the actions of the cannabinoid CBD on the TRPV2 channel. Despite the low efficacy of CBD relative to 2-APB as an agonist of rTRPV2, rTRPV1 and mTRPV3 channels, CBD sensitized all three channels to subsequent activation by 2-APB. However, sensitization in rTRPV2 and mTRPV3 channels was orders of magnitude stronger than in rTRPV1 channels. Our cryo-EM structural data for the full-length rTRPV2 in the presence of CBD and 2-APB confirmed the location of the CBD binding site ([Pumroy et al., 2019, 2022](#)) at the interface between the pore-domain, the membrane and the S4-S5 linker helix ([Figure 3](#)), and identified a second location where CBD can bind. The regions where CBD binds in rTRPV2 channels are highly conserved between TRPV1, TRPV2 and TRPV3 channels ([Figure 5](#) and [Figure 5 – Fig. Supplement 1](#)), and our mutagenesis results with rTRPV1 and rTRPV2 channels establish that the few residues that are not conserved between these channels are not determinant for the strength of the sensitization caused by CBD binding. Based on these findings, we propose that CBD interacts at similar locations in TRPV1 and TRPV2 channels, and speculate that this may also apply to TRPV3 channels. In contrast to the CBD site, the 2-APB binding sites proposed based on observations in TRPV3 ([Singh et al., 2018b; Zubcevic et al., 2019](#)) and TRPV2 ([Pumroy et al., 2022; Su et al., 2023](#)) channel structures lack sequence conservation, suggesting that the energetics of activation by 2-APB

could be very different in TRPV1, TRPV2 and TRPV3 channels, and could even involve distinct regions in each channel interacting with 2-APB. Importantly, we observed no evidence for 2-APB associated densities in our cryo-EM maps ([Figure 3 – Fig. Supplement 5](#)), calling for experimental clarification regarding the site or sites where 2-APB interacts with each of these channels.

We hypothesize that binding of CBD in rTRPV2 channels favors rearrangements on multiple sites in the protein that contribute energetically to activation by 2-APB without directly influencing the open-to-closed equilibrium, because CBD is such a low-efficacy agonist. Because binding of CBD sensitizes responses to 2-APB in rTRPV1 and rTRPV2 channels, albeit with different strength, it can be predicted that mutations at the site where CBD binds would significantly affect sensitivity to 2-APB by means of allosteric coupling. Indeed, we found that each of the positions we substituted had a minor influence on the sensitivity of rTRPV1 and rTRPV2 channels to CBD and a stronger influence on the sensitivity to 2-APB; further, each of the rTRPV1 channel mutants we examined affected sensitivity to 2-APB more strongly than to capsaicin ([Figure 6 – Fig. Supplement 1I](#)). Of note, rTRPV1 channels have an increased apparent affinity for 2-APB relative to rTRPV2 channels, with an EC₅₀ ~10-fold lower than that of rTRPV2 channels ([Figure 6G](#)). It can thus be hypothesized that the absence of strong

sensitization in rTRPV1 channels results from these channels already existing in a sensitized conformation ([Zubcevic et al., 2019](#)). Our mutagenesis results, however, show that the apparent affinity for 2-APB and sensitization by CBD are not strictly coupled in rTRPV1 channels: mutant M572V had an EC₅₀ for 2-APB that is similar in magnitude to WT rTRPV2 channels, and yet sensitization by CBD was completely absent, whereas the apparent 2-APB affinity for the triple mutant rTRPV1-M572V+C578L+M581L was so low that an EC₅₀ could not be determined, and yet responses to 2-APB were sensitized by CBD to the same extent as in WT rTRPV1 channels ([Figure 6G and andI](#)).[I](#).

Observations like this suggest a framework of TRPV channel function where the ensembles of conformational channel states stabilized by distinct agonists and allosteric modulators differ from each other at multiple significant locations throughout the protein, and that these differences, which could involve relatively subtle structural rearrangements, ultimately determine how the ensemble will respond to further challenges.

There appear to be many independent mechanisms through which TRPV2 channels can become sensitized to activation by 2-APB. Our results clearly indicate that sensitization caused by 2-APB itself ([Liu and Qin, 2016](#)) is over an order of magnitude weaker than that caused by CBD ([Figure 1G and andH](#)).[H](#)). This large difference

suggests that the ensemble of conformations adopted by the rTRPV2 channel when bound to CBD must have energetically significant differences from the set of conformations that predominate after channels become sensitized by a strong stimulation with 2-APB. As with 2-APB-dependent channel activation, the underlying molecular mechanism for 2-APB-dependent sensitization remains unknown. Sensitization by extreme heat increases the apparent affinity of rTRPV2 channels for 2-APB to a similar extent as CBD does, and also results in noticeable channel activity at ~40 °C ([Liu and Qin, 2016](#)). We didn't detect rTPRV2 channel activity at ~40 °C in the presence of CBD ([Figure 1 – Fig. Supplement 2](#)), indicating that CBD binding is not strongly coupled to heat-activation, and suggesting that the structural ensemble of heat-sensitized channels also bears significant differences at the energetic level from that of CBD-bound channels at temperatures below 40 °C. Interestingly, oxidative modification of two methionine residues in rTRPV2 channels strongly sensitized their responses to both heat and 2-APB ([Fricke et al., 2019](#)), indicating that methionine oxidation is less specific in its action than CBD, and suggesting that the underlying mechanism involves regions central to channel activation regardless of the stimulus.

In the case of mTRPV3 channels, we found that sensitization by 2-APB occurred much slower than by CBD, even when very high concentrations (3 mM) of 2-

~~ADD WORDS USED TO PRESENCE OF CHANNELS / FIGURE 1C~~ ✓

However, we also observed that current activation kinetics in the presence of CBD + 2-APB were similar to those after 2-APB-dependent sensitization (Figure 4G, ,HH and andK,K), suggesting that CBD-bound and 2-APB-sensitized apo mTRPV3 channels could adopt similar structural ensembles. It is unclear why CBD is so effective at sensitizing mTRPV3 channels without robustly activating them, whereas 2-APB can maximally activate channels but only after a slow sensitizing process – perhaps the CBD site is widely accessible in non-sensitized, apo mTRPV3 channels, whereas accessibility for 2-APB at the site that causes sensitization requires additional conformational rearrangements in the protein (and possibly the associated lipids ([Su et al., 2023](#))). The binding of CBD could rapidly sensitize channels by promoting these latter rearrangements and allowing 2-APB to access its sensitizing site. Importantly, the remarkably potent effect of CBD on mTRPV3 channel activation establishes it as a promising experimental manipulation that can help understand the unique kinetic features that characterize TRPV3 channel activation.

It will be interesting to test whether other molecules in addition to CBD can have similar effects on the sensitivity of TRPV2 and TRPV3 channels to 2-APB and possibly other agonists, especially because both ion channels have few known activators, endogenous or synthetic. Future drug or activator screens for TRPV2

and TRPV3 channels could benefit from combining test drugs together with low doses of 2-APB or CBD to determine whether non-linear additivity between ligands is a more general feature in these proteins.

Materials and Methods

Cell Culture

Human embryonic kidney cells (HEK293) from ATCC (CRL-1573) were kept at 37 °C in an atmosphere with 5% CO₂ and grown in Dulbecco's modified Eagle's medium (DMEM) with high glucose, pyruvate, L-glutamine, and phenol red, supplemented with 10% fetal bovine serum (vol/vol) and 10 mg/mL gentamicin. For transfection, cells were detached with trypsin, resuspended in DMEM and seeded onto No. 1 glass coverslips in 3 mL dishes at 10–40% confluency. Transfections were performed on the same day using FuGENE6 Transfection Reagent (Roche Applied Science, Madison, WI). TRP channel constructs were co-transfected with pGreen-Lantern (Invitrogen, Carlsbad, CA) at a ratio of 2:1 to visualize successfully transfected cells. Electrophysiological recordings were done 18–36 h after transfection.

Molecular biology

The WT rat TRPV1 ([Caterina et al., 1997](#)) and TRPV2 ([Caterina et al., 1999](#)) channel cDNA were provided by Dr. David Julius (UCSF, CA), and mouse TRPV3 ([Peier et al., 2002](#)) was provided by Dr. Fena Qin (SUNY Buffalo, NY).

All constructs were cloned into modified pcDNA3.1(+) and pcDNA1 for high and low levels of expression, respectively. CBD binding site mutants were generated using the two-step PCR method using Phusion High-Fidelity DNA polymerase (New England Biolabs, Ipswich MA), T4 ligase Quick Ligation kit (New England Biolabs) and NovaBlue Singles competent cells (MilliporeSigma, Burlington MA) and Sanger-sequenced to check for PCR errors. Cumulative pore mutants were generated by Gibson assembly (GeneArt Gibson Assembly kit, Thermo Fisher Scientific, Waltham MA) following manufacturer's instructions and using a gBlock (Integrated DNA Technologies, Coralville IA) encompassing nucleotides 1695-1993 in the rTRPV1 coding region.

Patch-clamp Electrophysiology

Patch clamp recordings were performed on transiently transfected HEK293 cells at room temperature (21–23°C) unless stated otherwise. Data were acquired with an Axopatch 200B amplifier (Molecular Devices, Sunnyvale, CA) and digitized with a Digidata1550B interface and pClamp10 software (Molecular Devices). All data were analyzed using Igor Pro 8.04 (Wavemetrics, Portland, OR). Pipettes were pulled from borosilicate glass (1.5 mm O.D. × 0.86 mm I.D. × 75 mm L; Harvard Apparatus) using a Sutter P-97 puller and heat-polished to final resistances between 0.5 and 4 MΩ using a MF-200 microforge (World Precision Instruments). 90% series resistance (R_s)

compensation was applied in all whole-cell recordings except those involving changes in temperature. An agar bridge (1M KCl; 4% weight/vol agar; teflon tubing) was used to connect the ground electrode chamber and the main recording chamber.

The extracellular solution consisted of (mM): 130 NaCl, 10 HEPES, 10 EGTA, pH 7.4 (NaOH/HCl). The same solution was used as the intracellular recording solution except for the addition of 10 $MgCl_2$, which was included to block endogenous inward-rectifying and low-threshold temperature-sensitive currents that were observed in some recordings. Stocks of 2-APB (1 M; Sigma-Aldrich, St. Louis, MO), CBD (10 mM; Cayman Chemical, Ann Arbor, MI) were prepared using DMSO, and capsaicin stock solutions (100 mM; Sigma-Aldrich) were prepared in ethanol. 2-APB stocks were prepared fresh every day, and CBD stocks were aliquoted and stored at -20°C, and diluted in recording solution immediately prior to recordings. The effective concentration of 2-APB in some of the most concentrated recording solutions that we used might be overestimated, because they were close to the solubility limit of the compound. Probenecid stock solution (100 mM) was made in 1 M NaOH, and used at a final concentration of 100 μ M in recording solution. We verified the pH of solutions using pH-indicator paper.

Whole-cell and excised-patch data using gap-free

recordings were acquired at 5 kHz and low-pass filtered at 1 kHz. Current-voltage (I-V) relations were acquired at 10 kHz and low-pass filtered at 2 kHz, and were obtained by applying 300 ms long voltage steps from a holding potential of 0 mV with a frequency of 1 Hz. Test pulses went from -100 to +100 mV in 10-mV increments. In all experiments at room temperature, a gravity-fed perfusion system (RSC-200, BioLogic, France) was used, in which outlets of glass capillaries were placed right in front of the recorded cells, and a motorized holder was used to switch between tube outlets. For rTRPV2 channel concentration-response relations for CBD and 2-APB in the presence and absence of CBD ([Figure 1E](#) and [and F](#)) we did not subtract background currents from the plotted data, which we normalized to the maximal concentration of either CBD (40 µM), 2-APB (4 mM) or 2-APB (4 mM) + 10 µM CBD. For the dose-response relations for WT and mutant rTRPV1 and rTRPV2 channels in [Supplementary Fig. 5](#), as well as group data from gap-free recordings and measurements of sensitization we subtracted the background currents measured in the absence of stimuli from the test currents before normalization. For normalization of the dose-response relations for 2-APB in some of the mutants we used the concentration that yielded maximal currents, because we observed pronounced channel desensitization at the highest concentrations in some of the mutants. Mean time-courses of mTRPV3 channel activation were obtained by aligning currents from each experiment to ~~the time in which cells were exposed to 2-APB for 2~~

second time (i.e. after the first exposure of 10 seconds duration that was used for normalization), segmented into intervals of 1.4 seconds duration (i.e. 7,000 data points), normalized, and averaged. All group data are shown as mean \pm SEM.

For single-channel recordings in the inside-out configuration, we acquired data at 10 kHz, low-pass filtered at 2 kHz, and we covered pipettes with dental wax to reduce capacitive transients and used pipettes with open tip resistances between 4–10 M Ω . Holding voltage was -80 mV, and 500 ms sweeps were recorded with a 100 ms inter-sweep interval, with 50 sweeps per patch in either control, 2-APB or CBD, and 2-APB and CBD applied together. All recorded traces were baseline-subtracted so that the mean current value in the absence of opening events was centered at 0 pA. The all-points histograms containing data from all sweeps per patch and experimental condition were normalized to the number of points at the peak centered at 0 pA, and binned using of 0.2 pA intervals.

Experiments involving temperature increases were carried out using a custom-built device as previously described ([Islas et al., 2015; Sánchez-Moreno et al., 2018](#)), which consists of using a wire-based microheater enclosed in a glass pipette for insulation and connected to a power source for heating. For our device we used 0.1 mm diameter nichrome wire connected to a Keysight Technologies (Santa Rosa, CA)

E3631A Triple Output DC Power Supply. Maximum output was utilized from the power supply, which was approximately 6 V and 0.74 A. The wire was introduced into a glass capillary pipette, which was bent to a U-shape using a flame. The U-shaped pipette with the wire inside connected to the power source was held on a micro-manipulator and placed right in front of the patch pipette inside the recording chamber. To estimate the changes in temperature achieved by our heating device, we used the resistance measured from an open patch pipette, whose resistance measurements as a function of heating were previously calibrated by exchanging the recording bath with solutions at multiple temperatures, which we measured with a thermistor (Warner TC-324B, Hamden, CT) placed close to the pipette tip inside the bath. The heating device was then placed at a defined distance from the same pipette tip and the pipette resistance measured after turning the power supply on with maximal output for 90 s. For each calibration, we measured the pipette resistance R as a function of temperature and fit the data to $R(\text{Temp}) = R_0 \times \exp(A_0/\text{Temp})$ (Equation 1), where the fit parameters R_0 and A_0 are constants specific for each pipette. From Eq. 1 we obtained the temperature (Temp) as a function of resistance: $\text{Temp} = A_0 / [\ln(R) - \ln(R_0)]$ (Equation 2). We then introduced the heating device and recorded resistance as a function of time at full power source output for 90 s, and fitted the resulting function to a double-exponential function of time: $R(\text{time}) =$

$R(\text{time}=0) + A_1 \times \exp(-\text{time} \times k_1) + A_2 \times \exp(-\text{time} \times k_2)$ (Equation 3), where the fitted parameters A_1 , A_2 , k_1 , k_2 , are constants specific to each heating device and its relative position to the tip of the pipette. The other fit parameter $R(\text{time} = 0)$ depends entirely on the pipette, and is equivalent to R_0 in Eq. 2 – the resistance of the pipette at the room temperature of 21 °C. We obtained reproducible fitting parameters for the exponential using different pipettes with the same heating device, suggesting a highly reproducible time-dependent increase in temperature. To estimate the average temperature change during each experiment, we expressed Eq. 2 in terms of Eq. 3: $\text{Temp}(\text{time}) = A_0 / [\ln(R(\text{time})) - \ln(R_0)]$ (Equation 4), and plotted our currents as a function of temperature by transforming recording time into temperature using Equation 4 and the mean fit parameters for the exponential terms that we obtained from several trials with the same heating device and different open pipettes ($n = 15$). Based on this high reproducibility, we assume that the time-dependence and magnitude of the temperature change was similar in all experiments, and thus used the same parameters for all experiments. Q_{10} values were calculated by taking the logarithm of current-temperature relations from individual experiments, fitting them to a line with slope m over the range from 30–40 °C, and then using Equation 5: $Q_{10} = 10^{10} \times m$.

High-performance liquid chromatography

Samples were prepared using our regular recordings solution without adding trifluoroacetic acid to maintain a neutral pH. We injected 50 nmol of 2-APB and 5 nmol of CBD, either by themselves or together, and the final volume injected into the HPLC column was 400 µL with the compound diluted in dH₂O. We injected samples into a 5µM Ultrasphere C18 column (Beckman Coulter, Brea CA) on a 1525 Binary pump HPLC system (Waters Corporation, Milford MA), and used a gradient of 0% to 100% acetonitrile over 40 minutes and monitored sample absorbance at 228 nm.

Sequence alignment and structural model depiction

We generated our amino acid sequence alignments using Jalview software (University of Dundee).

rTRPV2 channel expression using Baculovirus and mammalian expression system

To produce the rTRPV2 channel for cryo-EM, the channel was cloned into the pEG vector in which EGFP was substituted with mVenus ([Rana et al., 2018](#)) and expressed in tsA201 cells using the previously published Baculovirus-mammalian expression system with a few minor modifications ([Goehring et al., 2014](#)).

Briefly, P1 virus was generated by transfecting Sf9 cells (~2.5 million cells on a T25 flask with a vent cap) with 50 – 100 ng of fresh Bacmid using Cellfectin. After 4 – 5 days incubation in a humidified 28 °C incubator, the cell culture media was collected by centrifugation (3,000g × 10 min), supplemented with 2% FBS, and

filtered through a 0.45 µm filter to harvest the P1 virus. To amplify the P1 virus, ~500 ml Sf9 cell cultures at a ~1.5 million cells/ml density were infected with 1 – 200 µl of the virus and incubated in a 28 °C shaking incubator for 3 days. The cell culture media was then collected by centrifugation (5,000g × 20 min), supplemented with 2% FBS, and filter through 0.45 µm filter to harvest P2 virus. The volume of P1 virus used for the amplification was determined by carrying out a small-scale amplification screening in which ~10 ml Sf9 cell cultures at the same density were infected with different volume of P1 virus and harvested after 3 days to transduce tsA201 cells and compare the expression level of rTRPV2 using mVenus fluorescence intensity. The P2 virus was protected from light using aluminum foil and stored at 4 °C until use. To express the rTRPV2, tsA201 cells at ~1.5 million cells/ml in Freestyle medium with 2 % FBS were transduced with 10 % (v/v) P2 virus and incubated at a 37 °C CO₂ incubator. To boost the protein expression, sodium butyrate (2 M stock in H₂O) was added to 10 mM at ~16 hours of post-transduction. The culture was continued at the 37 °C CO₂ incubator for another 24 hours, and the cells were harvested by centrifugation (5,000g × 20 min) and frozen at –80 °C until use.

rTRPV2 channel purification

Prior to extraction of rTRPV2 from tsA201 cells, membrane fractionation was carried out using a hypotonic solution and ultracentrifugation. The cells

were first resuspended in a hypotonic solution (20 mM

Tris pH 7.5 and 10 mM NaCl) with protease inhibitors (pepstatin, aprotinin, leupeptin, benzamidine, trypsin inhibitor, PMFS) using a Dounce homogenizer, incubated at 4 °C for ~30 minutes, and centrifuged at 1,000 g for 10 minutes to remove cell debris. The supernatant was ultracentrifuged for 1 hour (45,000 rpm, Beckman Ti45 rotor) and collected membranes were stored at –80 °C until use. To purify rTRPV2, the fractionated membranes were resuspended in an extraction buffer (50 mM Tris pH 7.5, 150 mM NaCl, 5% glycerol, 2 mM TCEP, 50 mM DDM, 5 mM CHS with the protease inhibitor mixture used above) and extracted for 1 hour at 4 °C. The solution was clarified by centrifugation (12,000g × 10 min) and incubated with CoTALON resins at 4 °C for 1 hour, at which point the mixture was transferred to an empty disposable column (Econo-Pac® Biorad). The resin was washed with 10 column volume of Buffer A (50 mM Tris pH 7.5, 150 mM NaCl, 1 mM DDM, 0.1 mM CHS, and 0.1 mg/ml porcine brain total lipid extract) with 10 mM imidazole, and bound proteins were eluted with Buffer A with 250 mM imidazole. The eluate was concentrated using Amicon Ultra (100kDa) to ~350 – 450 µl and loaded onto a Superose6 (10×300mm) gel filtration column and separated with Buffer A. All purification steps described above was carried out at 4 °C or on ice.

Lipid nanodisc reconstitution of the rTRPV2 channel

Lipid nanodisc reconstitution was performed following the previously published methods with minor

modifications ([Matthies et al., 2018](#); [Tan et al., 2022](#)). On the day of nanodisc reconstitution, the rTRPV2 channel purified by Superose6 in detergent was concentrated to ~1–3 mg/ml and incubated with histidine tagged MSP1E3D1 and 3:1:1 mixture of 1-palmitoyl-2-oleoyl-sn-glycero-3-phosphocholine (POPC), 1-palmitoyl-2-oleoyl-sn-glycero-3-phospho-(1'-rac-glycerol) (POPG) and 1-palmitoyl-2-oleoyl-sn-glycero-3-phosphoethanolamine (POPE) for 30 minutes at room temperature. The mixture was transferred to a tube with Biobeads (~30–50 fold of detergent; w/w) and incubated at room temperature for ~3 hours in the presence of TEV protease (prepared in-house) and 2 mM TCEP to remove N-terminal fusion protein including poly-histidine and mVenus tag. The reconstituted protein was loaded onto Superose6 column (10×300mm) and separated using 20 mM Tris and 150 mM NaCl buffer at 4 °C. The success of nanodisc reconstitution was confirmed by collecting separated fractions and running SDS-PAGE to verify the presence of rTRPV2 and MSP1E3D1 bands at a similar ratio. Typically, optimal reconstitution required the incubation of 1:10:200 or 1:10:400 molar ratio of tetrameric rTRPV2, MSP1E3D1, and the lipid mixture.

Cryo-EM sample preparation and data acquisition

6.5 mg/ml TRPV2 in nanodiscs were incubated with 100 µM CBD and 1 mM 2-APB on ice for 30 min and then 3 µL aliquots were applied to glow-discharged Quantifoil grids (R 1 2/1 3 Cu 300 mesh). The grids

were blotted for 4 s, with blot force of 4 and 100% humidity, at 16°C using an FEI Vitrobot Mark IV (Thermo Fisher Scientific), followed by plunging into liquid ethane cooled by liquid nitrogen. Images were acquired using an FEI Titan Krios equipped with a Gatan LS image energy filter (slit width, 20 eV) operating at 300 kV. A Gatan K3 Summit direct electron detector was used to record movies in superresolution mode with a nominal magnification of $\times 105,000$, resulting in a calibrated pixel size of 0.43 Å per pixel. The typical defocus values ranged from –0.5 to –1.5 μm. Exposures of 1.6 s were dose-fractionated into 32 frames, resulting in a total dose of 52 e[–] Å^{–2}. Images were recorded using the automated acquisition program SerialEM ([Mastronarde, 2005](#)).

Image processing

All processing was completed in RELION ([Mastronarde, 2005](#)). The beam-induced image motion between frames of each dose-fractionated micrograph was corrected and binned by 2 using MotionCor2 ([Zheng et al., 2017](#)) and contrast transfer function (CTF) estimation was performed using CTFFIND4 ([Rohou and Grigorieff, 2015](#)). Micrographs were selected, and those with outliers in defocus value and astigmatism, as well as low resolution (>5 Å) reported by CTFFIND4 were removed. The initial set of particles from 300 micrographs were picked using Gautomatch

(www2.mrc-lmb.cam.ac.uk/research/locally-developed-software/zhang-software/#gauto) and followed by reference-free two-dimensional (2D) classification in RELION. The good classes were then used as template to pick particles from all selected micrographs using Gautomatch. Particles (1,665,271) were picked and extracted with 2× downscaling (pixel size, 1.72 Å). Several rounds of reference-free 2D classification were performed to remove ice spot, contaminants, and bad particles. The good particles were 3D classified with C4 symmetry using reference generated by 3D initial model. Good class (380,829) were then selected and reextracted without binning (pixel size, 0.86 Å) followed by 3D auto-refine. After that, the refined particles were expanded from C4 symmetry to C1 symmetry and then subjected to 3D Classification (skip alignment) with transmembrane domain mask. 6 classes show one CBD binding site in each monomer (conformation A) and one class shows two CBD binding sites per monomer (conformation B). Particles (1,370,377) from these 6 classes were combined and duplication was removed. Finally, 322,102 unique particles were obtained and submitted to final step of 3D auto-refine with C4 symmetry. Particles (43,071) from conformation B were selected by removing duplication followed by 3D auto-refine. The final reconstruction was reported at 3.26 Å for conformation A and 3.44 Å for conformation B.

Model building and structure refinement

Model building was first carried out by manually fitting the monomer of rTRPV2 (PDB 6U84) into the electron microscopy density map using UCSF Chimera ([Pettersen et al., 2004](#)). The model was then manually built in Coot ([Emsley et al., 2010](#)) and refined using real space refinement in PHENIX ([Adams et al., 2010](#)) with secondary structure and geometry restraints. The final model was evaluated by comprehensive validation in PHENIX. Structural figures were generated using PyMOL (<https://pymol.org/2/support.html>) and UCSF Chimera.

Acknowledgements

We thank Rick Aldrich, Eric Senning and Marcel Goldschen-Ohm for helpful discussions and León D. Islas and Ernesto Ladrón-de-Guevara for discussions in building the heating device. This research was supported startup funds from the University of Texas at Austin (to AJO), NINDS R00 Career Development Award 4R00NS101053-02 (to AJO), and the Intramural Research Programs of the NINDS (to KJS).

Data and Materials Availability

All data needed to evaluate the conclusions in the paper are present in the paper, the Supplementary Materials, or uploaded as Source data. Maps for conformations A and B for rTRPV2 have been deposited in the Electron Microscopy Data Bank (EMDB) under accession codes EMD-29526 and EMD-29532, respectively. Models of conformations A and B

for rTRPV2 have been deposited in the Protein Data Bank with accession codes 8FX8 and 8FXG, respectively.

References

- Adams P. D.; Afonine P. V.; Bunkóczki G.; Chen V. B.; Davis I. W.; Echols N.; Headd J. J.; Hung L.-W.; Kapral G. J.; Grosse-Kunstleve R. W.; et al. PHENIX: A Comprehensive Python-Based System for Macromolecular Structure Solution. *Acta Crystallogr. D Biol. Crystallogr.* 2010, 66, 213–221. [[PMC free article](#)] [[PubMed](#)] [[Google Scholar](#)]
- Bai D.; del Corso C.; Srinivas M.; Spray D. C. Block of Specific Gap Junction Channel Subtypes by 2-Aminoethoxydiphenyl Borate (2-APB). *J. Pharmacol. Exp. Ther.* 2006, 319, 1452–1458. [[PubMed](#)] [[Google Scholar](#)]
- Bang S.; Kim K. Y.; Yoo S.; Lee S.-H.; Hwang S. W. Transient Receptor Potential V2 Expressed in Sensory Neurons Is Activated by Probenecid. *Neurosci. Lett.* 2007, 425, 120–125. [[PubMed](#)] [[Google Scholar](#)]
- Belkacemi A.; Trost C. F.; Tinschert R.; Flormann D.; Malihpour M.; Wagner C.; Meyer M. R.; Beck A.; Flockerzi V. The TRPV2 Channel Mediates Ca²⁺ Influx and the Δ9-THC-Dependent Decrease in Osmotic Fragility in Red Blood Cells. *Haematologica* 2021, 106, 2246–2250. [[PMC free article](#)] [[PubMed](#)] [[Google Scholar](#)]
- Bisogno T.; Hanus L.; De Petrocellis L.; Tchilibon S.; Ponde D. E.; Brandi I.; Moriello A. S.; Davis J. B.; Mechoulam R.; Di Marzo V. Molecular Targets for Cannabidiol and Its Synthetic Analogue: Effect on Vanilloid VR1 Receptors and on the Cellular Uptake and Enzymatic Hydrolysis of Anandamide. *Br. J. Pharmacol.* 2001, 134, 845–852. [[PMC free article](#)] [[PubMed](#)] [[Google Scholar](#)]
- Bohlen C. J.; Priel A.; Zhou S.; King D.; Siemens J.:

Julius D. A Bivalent Tarantula Toxin Activates the Capsaicin Receptor, TRPV1, by Targeting the Outer Pore Domain. *Cell* 2010, 141, 834–845. [[PMC free article](#)] [[PubMed](#)] [[Google Scholar](#)]

- Bootman M. D.; Collins T. J.; Mackenzie L.; Roderick H. L.; Berridge M. J.; Peppiatt C. M. 2-Aminoethoxydiphenyl Borate (2-APB) Is a Reliable Blocker of Store-Operated Ca²⁺ Entry but an Inconsistent Inhibitor of InsP₃-Induced Ca²⁺ Release. *FASEB J.* 2002, 16, 1145–1150. [[PubMed](#)] [[Google Scholar](#)]
- Canul-Sánchez J. A.; Hernández-Araiza I.; Hernández-García E.; Llorente I.; Morales-Lázaro S. L.; Islas L. D.; Rosenbaum T. Different Agonists Induce Distinct Single-Channel Conductance States in TRPV1 Channels. *J. Gen. Physiol.* 2018, 150, 1735–1746. [[PMC free article](#)] [[PubMed](#)] [[Google Scholar](#)]
- Caterina M. J.; Schumacher M. A.; Tominaga M.; Rosen T. A.; Levine J. D.; Julius D. The Capsaicin Receptor: A Heat-Activated Ion Channel in the Pain Pathway. *Nature* 1997, 389, 816–824. [[PubMed](#)] [[Google Scholar](#)]
- Caterina M. J.; Rosen T. A.; Tominaga M.; Brake A. J.; Julius D. A Capsaicin-Receptor Homologue with a High Threshold for Noxious Heat. *Nature* 1999, 398, 436–441. [[PubMed](#)] [[Google Scholar](#)]
- Deng Z.; Maksaev G.; Rau M.; Xie Z.; Hu H.; Fitzpatrick J. A. J.; Yuan P. Gating of Human TRPV3 in a Lipid Bilayer. *Nat. Struct. Mol. Biol.* 2020, 27, 635–644. [[PMC free article](#)] [[PubMed](#)] [[Google Scholar](#)]
- De Petrocellis L.; Orlando P.; Moriello A. S.; Aviello G.; Stott C.; Izzo A. A.; Di Marzo V. Cannabinoid Actions at TRPV Channels: Effects on TRPV3 and TRPV4 and Their Potential Relevance to Gastrointestinal Inflammation. *Acta Physiol (Oxf)* 2012, 204, 255–266. [[PubMed](#)] [[Google Scholar](#)]
- Emsley P.; Lohkamp B.; Scott W. G.; Cowtan K. Features and Development of Coot. *Acta Crystallogr. D Biol. Crystallogr.* 2010, 66, 486–501. [[PMC free article](#)] [[PubMed](#)] [[Google Scholar](#)]

- Fricke T. C.; Echtermeyer F.; Zielke J.; de la Roche J.; Filipovic M. R.; Claverol S.; Herzog C.; Tominaga M.; Pumroy R. A.; Moiseenkova-Bell V. Y.; et al. Oxidation of Methionine Residues Activates the High-Threshold Heat-Sensitive Ion Channel TRPV2. *Proc Natl Acad Sci USA* 2019, 116, 24359–24365. [[PMC free article](#)] [[PubMed](#)] [[Google Scholar](#)]
- Gao L.; Yang P.; Qin P.; Lu Y.; Li X.; Tian Q.; Li Y.; Xie C.; Tian J.; Zhang C.; et al. Selective Potentiation of 2-APB-Induced Activation of TRPV1–3 Channels by Acid. *Sci. Rep.* 2016a, 6, 20791. [[PMC free article](#)] [[PubMed](#)] [[Google Scholar](#)]
- Gao Y.; Cao E.; Julius D.; Cheng Y. TRPV1 Structures in Nanodiscs Reveal Mechanisms of Ligand and Lipid Action. *Nature* 2016b, 534, 347–351. [[PMC free article](#)] [[PubMed](#)] [[Google Scholar](#)]
- Geron M.; Kumar R.; Zhou W.; Faraldo-Gómez J. D.; Vásquez V.; Priel A. TRPV1 Pore Turret Dictates Distinct DkTx and Capsaicin Gating. *Proc Natl Acad Sci USA* 2018, 115, E11837–E11846. [[PMC free article](#)] [[PubMed](#)] [[Google Scholar](#)]
- Goehring A.; Lee C.-H.; Wang K. H.; Michel J. C.; Claxton D. P.; Baconguis I.; Althoff T.; Fischer S.; Garcia K. C.; Gouaux E. Screening and Large-Scale Expression of Membrane Proteins in Mammalian Cells for Structural Studies. *Nat. Protoc.* 2014, 9, 2574–2585. [[PMC free article](#)] [[PubMed](#)] [[Google Scholar](#)]
- Grandl J.; Hu H.; Bandell M.; Bursulaya B.; Schmidt M.; Petrus M.; Patapoutian A. Pore Region of TRPV3 Ion Channel Is Specifically Required for Heat Activation. *Nat. Neurosci.* 2008, 11, 1007–1013. [[PMC free article](#)] [[PubMed](#)] [[Google Scholar](#)]
- Grandl J.; Kim S. E.; Uzzell V.; Bursulaya B.; Petrus M.; Bandell M.; Patapoutian A. Temperature-Induced Opening of TRPV1 Ion Channel Is Stabilized by the Pore Domain. *Nat. Neurosci.* 2010, 13, 708–714. [[PMC free article](#)] [[PubMed](#)] [[Google Scholar](#)]
- Guéguinou M.; Felix R.; Marionneau-Lambot S.;

Y.; Ternant D.; Arnoult C.; et al. Synthetic Alkyl-Ether-Lipid Promotes TRPV2 Channel Trafficking Through PI3K/Akt-Girdin Axis in Cancer Cells and Increases Mammary Tumour Volume. *Cell Calcium* 2021, 97, 102435. [\[PubMed\]](#) [\[Google Scholar\]](#)

- Hisanaga E.; Nagasawa M.; Ueki K.; Kulkarni R. N.; Mori M.; Kojima I. Regulation of Calcium-Permeable TRPV2 Channel by Insulin in Pancreatic Beta-Cells. *Diabetes* 2009, 58, 174–184. [\[PMC free article\]](#) [\[PubMed\]](#) [\[Google Scholar\]](#)
- Huynh K. W.; Cohen M. R.; Jiang J.; Samanta A.; Lodowski D. T.; Zhou Z. H.; Moiseenkova-Bell V. Y. Structure of the Full-Length TRPV2 Channel by Cryo-EM. *Nat. Commun.* 2016, 7, 11130. [\[PMC free article\]](#) [\[PubMed\]](#) [\[Google Scholar\]](#)
- Hu H.-Z.; Gu Q.; Wang C.; Colton C. K.; Tang J.; Kinoshita-Kawada M.; Lee L.-Y.; Wood J. D.; Zhu M. X. 2-Aminoethoxydiphenyl Borate Is a Common Activator of TRPV1, TRPV2, and TRPV3. *J. Biol. Chem.* 2004, 279, 35741–35748. [\[PubMed\]](#) [\[Google Scholar\]](#)
- Hwang S. W.; Cho H.; Kwak J.; Lee S. Y.; Kang C. J.; Jung J.; Cho S.; Min K. H.; Suh Y. G.; Kim D.; et al. Direct Activation of Capsaicin Receptors by Products of Lipoxygenases: Endogenous Capsaicin-like Substances. *Proc Natl Acad Sci USA* 2000, 97, 6155–6160. [\[PMC free article\]](#) [\[PubMed\]](#) [\[Google Scholar\]](#)
- Iannotti F. A.; Hill C. L.; Leo A.; Alhusaini A.; Soubrane C.; Mazzarella E.; Russo E.; Whalley B. J.; Di Marzo V.; Stephens G. J. Nonpsychotropic Plant Cannabinoids, Cannabidivarin (CBDV) and Cannabidiol (CBD), Activate and Desensitize Transient Receptor Potential Vanilloid 1 (TRPV1) Channels in Vitro: Potential for the Treatment of Neuronal Hyperexcitability. *ACS Chem. Neurosci.* 2014, 5, 1131–1141. [\[PubMed\]](#) [\[Google Scholar\]](#)
- Islas L. D.; De-la-Rosa V.; Rodríguez-Cortés B.; Rangel-Yescas G. E.; Elias-Viñas D. A Simple Method

Thermal Activation of TRPV1 Ion Channels. *J. Neurosci. Methods* 2015, 243, 120–125. [[PubMed](#)] [[Google Scholar](#)]

- Iwata Y.; Matsumura T. Blockade of TRPV2 Is a Novel Therapy for Cardiomyopathy in Muscular Dystrophy. *Int. J. Mol. Sci.* 2019, 20. [[PMC free article](#)] [[PubMed](#)] [[Google Scholar](#)]
- Jara-Oseguera A.; Bae C.; Swartz K. J. An External Sodium Ion Binding Site Controls Allosteric Gating in TRPV1 Channels. *eLife* 2016, 5. [[PMC free article](#)] [[PubMed](#)] [[Google Scholar](#)]
- Jara-Oseguera A.; Huffer K. E.; Swartz K. J. The Ion Selectivity Filter Is Not an Activation Gate in TRPV1–3 Channels. *eLife* 2019, 8. [[PMC free article](#)] [[PubMed](#)] [[Google Scholar](#)]
- Jordt S. E.; Tominaga M.; Julius D. Acid Potentiation of the Capsaicin Receptor Determined by a Key Extracellular Site. *Proc Natl Acad Sci USA* 2000, 97, 8134–8139. [[PMC free article](#)] [[PubMed](#)] [[Google Scholar](#)]
- Joseph J.; Qu L.; Wang S.; Kim M.; Bennett D.; Ro J.; Caterina M. J.; Chung M.-K. Phosphorylation of TRPV1 S801 Contributes to Modality-Specific Hyperalgesia in Mice. *J. Neurosci.* 2019, 39, 9954–9966. [[PMC free article](#)] [[PubMed](#)] [[Google Scholar](#)]
- Juvin V.; Penna A.; Chemin J.; Lin Y.-L.; Rassendren F.-A. Pharmacological Characterization and Molecular Determinants of the Activation of Transient Receptor Potential V2 Channel Orthologs by 2-Aminoethoxydiphenyl Borate. *Mol. Pharmacol.* 2007, 72, 1258–1268. [[PubMed](#)] [[Google Scholar](#)]
- Katanosaka Y.; Iwasaki K.; Ujihara Y.; Takatsu S.; Nishitsuji K.; Kanagawa M.; Sudo A.; Toda T.; Katanosaka K.; Mohri S.; et al. TRPV2 Is Critical for the Maintenance of Cardiac Structure and Function in Mice. *Nat. Commun.* 2014, 5, 3932. [[PMC free article](#)] [[PubMed](#)] [[Google Scholar](#)]
- Kovacs G.; Montalbetti N.; Simonin A.; Danko T.; Balazs B.; Zsembery A.; Hediger M. A. Inhibition of

Cannabidiol sensitizes TRPV2 channels to activation by 2-APB
the Human Epithelial Calcium Channel TRPV6 by 2-

Aminoethoxydiphenyl Borate (2-APB). Cell Calcium 2012, 52, 468–480. [[PubMed](#)] [[Google Scholar](#)]

- Kudou M.; Shiozaki A.; Yamazato Y.; Katsurahara K.; Kosuga T.; Shoda K.; Arita T.; Konishi H.; Komatsu S.; Kubota T.; et al. The Expression and Role of TRPV2 in Esophageal Squamous Cell Carcinoma. Sci. Rep. 2019, 9, 16055. [[PMC free article](#)] [[PubMed](#)] [[Google Scholar](#)]
- Lévêque M.; Penna A.; Le Trionnaire S.; Belleguic C.; Desrues B.; Brinchault G.; Jouneau S.; Lagadic-Gossmann D.; Martin-Chouly C. Phagocytosis Depends on TRPV2-Mediated Calcium Influx and Requires TRPV2 in Lipids Rafts: Alteration in Macrophages from Patients with Cystic Fibrosis. Sci. Rep. 2018, 8, 4310. [[PMC free article](#)] [[PubMed](#)] [[Google Scholar](#)]
- Ligresti A.; Moriello A. S.; Starowicz K.; Matias I.; Pisanti S.; De Petrocellis L.; Laezza C.; Portella G.; Bifulco M.; Di Marzo V. Antitumor Activity of Plant Cannabinoids with Emphasis on the Effect of Cannabidiol on Human Breast Carcinoma. J. Pharmacol. Exp. Ther. 2006, 318, 1375–1387. [[PubMed](#)] [[Google Scholar](#)]
- Link T. M.; Park U.; Vonakris B. M.; Raben D. M.; Soloski M. J.; Caterina M. J. TRPV2 Has a Pivotal Role in Macrophage Particle Binding and Phagocytosis. Nat. Immunol. 2010, 11, 232–239. [[PMC free article](#)] [[PubMed](#)] [[Google Scholar](#)]
- Liu B.; Qin F. Use Dependence of Heat Sensitivity of Vanilloid Receptor TRPV2. Biophys. J. 2016, 110, 1523–1537. [[PMC free article](#)] [[PubMed](#)] [[Google Scholar](#)]
- Liu B.; Yao J.; Zhu M. X.; Qin F. Hysteresis of Gating Underlines Sensitization of TRPV3 Channels. J. Gen. Physiol. 2011, 138, 509–520. [[PMC free article](#)] [[PubMed](#)] [[Google Scholar](#)]
- Mastronarde D. N. Automated Electron Microscope Tomography Using Robust Prediction of Specimen Movements. J. Struct. Biol. 2005, 152, 36–51.

[\[PubMed\]](#) [\[Google Scholar\]](#)

- Matthies D.; Bae C.; Toombes G. E.; Fox T.; Bartesaghi A.; Subramaniam S.; Swartz K. J. Single-Particle Cryo-EM Structure of a Voltage-Activated Potassium Channel in Lipid Nanodiscs. *eLife* 2018, 7. [\[PMC free article\]](#) [\[PubMed\]](#) [\[Google Scholar\]](#)
- Monet M.; Lehen'kyi V.; Gackiere F.; Firlej V.; Vandenberghe M.; Roudbaraki M.; Gkika D.; Pourtier A.; Bidaux G.; Slomiany C.; et al. Role of Cationic Channel TRPV2 in Promoting Prostate Cancer Migration and Progression to Androgen Resistance. *Cancer Res.* 2010, 70, 1225–1235. [\[PubMed\]](#) [\[Google Scholar\]](#)
- Neeper M. P.; Liu Y.; Hutchinson T. L.; Wang Y.; Flores C. M.; Qin N. Activation Properties of Heterologously Expressed Mammalian TRPV2: Evidence for Species Dependence. *J. Biol. Chem.* 2007, 282, 15894–15902. [\[PubMed\]](#) [\[Google Scholar\]](#)
- Nieto-Posadas A.; Picazo-Juárez G.; Llorente I.; Jara-Oseguera A.; Morales-Lázaro S.; Escalante-Alcalde D.; Islas L. D.; Rosenbaum T. Lysophosphatidic Acid Directly Activates TRPV1 through a C-Terminal Binding Site. *Nat. Chem. Biol.* 2011, 8, 78–85. [\[PubMed\]](#) [\[Google Scholar\]](#)
- Pauli C. S.; Conroy M.; Vanden Heuvel B. D.; Park S.-H. Cannabidiol Drugs Clinical Trial Outcomes and Adverse Effects. *Front. Pharmacol.* 2020, 11, 63. [\[PMC free article\]](#) [\[PubMed\]](#) [\[Google Scholar\]](#)
- Peier A. M.; Reeve A. J.; Andersson D. A.; Moqrich A.; Earley T. J.; Hergarden A. C.; Story G. M.; Colley S.; Hogenesch J. B.; McIntyre P.; et al. A Heat-Sensitive TRP Channel Expressed in Keratinocytes. *Science* 2002, 296, 2046–2049. [\[PubMed\]](#) [\[Google Scholar\]](#)
- Pettersen E. F.; Goddard T. D.; Huang C. C.; Couch G. S.; Greenblatt D. M.; Meng E. C.; Ferrin T. E. UCSF Chimera—a Visualization System for Exploratory Research and Analysis. *J. Comput. Chem.* 2004, 25, 1605–1612. [\[PubMed\]](#) [\[Google Scholar\]](#)
- Pumroy R. A.; Samanta A.; Liu Y.; Hughes T. E.; Zhao S.; Yudin Y.; Rohacs T.; Han S.; Moiseenkova-Bell V.

Y. Molecular Mechanism of TRPV2 Channel

Modulation by Cannabidiol. *eLife* 2019, 8. [[PMC free article](#)] [[PubMed](#)] [[Google Scholar](#)]

- Pumroy R. A.; Protopopova A. D.; Fricke T. C.; Lange I. U.; Haug F. M.; Nguyen P. T.; Gallo P. N.; Sousa B. B.; Bernardes G. J. L.; Yarov-Yarovoy V.; et al. Structural Insights into TRPV2 Activation by Small Molecules. *Nat. Commun.* 2022, 13, 2334. [[PMC free article](#)] [[PubMed](#)] [[Google Scholar](#)]
- Qin N.; Neeper M. P.; Liu Y.; Hutchinson T. L.; Lubin M. L.; Flores C. M. TRPV2 Is Activated by Cannabidiol and Mediates CGRP Release in Cultured Rat Dorsal Root Ganglion Neurons. *J. Neurosci.* 2008, 28, 6231–6238. [[PMC free article](#)] [[PubMed](#)] [[Google Scholar](#)]
- Rana M. S.; Wang X.; Banerjee A. An Improved Strategy for Fluorescent Tagging of Membrane Proteins for Overexpression and Purification in Mammalian Cells. *Biochemistry* 2018, 57, 6741–6751. [[PMC free article](#)] [[PubMed](#)] [[Google Scholar](#)]
- Rohou A.; Grigorieff N. CTFFIND4: Fast and Accurate Defocus Estimation from Electron Micrographs. *J. Struct. Biol.* 2015, 192, 216–221. [[PMC free article](#)] [[PubMed](#)] [[Google Scholar](#)]
- Salazar H.; Llorente I.; Jara-Oseguera A.; García-Villegas R.; Munari M.; Gordon S. E.; Islas L. D.; Rosenbaum T. A Single N-Terminal Cysteine in TRPV1 Determines Activation by Pungent Compounds from Onion and Garlic. *Nat. Neurosci.* 2008, 11, 255–261. [[PMC free article](#)] [[PubMed](#)] [[Google Scholar](#)]
- Sánchez-Moreno A.; Guevara-Hernández E.; Contreras-Cervera R.; Rangel-Yescas G.; Ladrón-de-Guevara E.; Rosenbaum T.; Islas L. D. Irreversible Temperature Gating in Trpv1 Sheds Light on Channel Activation. *eLife* 2018, 7. [[PMC free article](#)] [[PubMed](#)] [[Google Scholar](#)]
- Shimada H.; Kusakizako T.; Dung Nguyen T. H.; Nishizawa T.; Hino T.; Tominaga M.; Nureki O. The Structure of Lipid Nanodisc-Reconstituted TRPV3

- Reveals the Gating Mechanism. *Nat. Struct. Mol. Biol.* 2020, 27, 645–652. [[PubMed](#)] [[Google Scholar](#)]
- Shin J.; Cho H.; Hwang S. W.; Jung J.; Shin C. Y.; Lee S.-Y.; Kim S. H.; Lee M. G.; Choi Y. H.; Kim J.; et al. Bradykinin-12-Lipoxygenase-VR1 Signaling Pathway for Inflammatory Hyperalgesia. *Proc Natl Acad Sci USA* 2002, 99, 10150–10155. [[PMC free article](#)] [[PubMed](#)] [[Google Scholar](#)]
 - Singh A. K.; Saotome K.; McGoldrick L. L.; Sobolevsky A. I. Structural Bases of TRP Channel TRPV6 Allosteric Modulation by 2-APB. *Nat. Commun.* 2018a, 9, 2465. [[PMC free article](#)] [[PubMed](#)] [[Google Scholar](#)]
 - Singh A. K.; McGoldrick L. L.; Sobolevsky A. I. Structure and Gating Mechanism of the Transient Receptor Potential Channel TRPV3. *Nat. Struct. Mol. Biol.* 2018b, 25, 805–813. [[PMC free article](#)] [[PubMed](#)] [[Google Scholar](#)]
 - Siveen K. S.; Nizamuddin P. B.; Uddin S.; Al-Thani M.; Frenneaux M. P.; Janahi I. A.; Steinhoff M.; Azizi F. TRPV2: A Cancer Biomarker and Potential Therapeutic Target. *Dis. Markers* 2020, 2020, 8892312. [[PMC free article](#)] [[PubMed](#)] [[Google Scholar](#)]
 - Su N.; Zhen W.; Zhang H.; Xu L.; Jin Y.; Chen X.; Zhao C.; Wang Q.; Wang X.; Li S.; et al. Structural Mechanisms of TRPV2 Modulation by Endogenous and Exogenous Ligands. *Nat. Chem. Biol.* 2023, 19, 72–80. [[PubMed](#)] [[Google Scholar](#)]
 - Tamura S.; Morikawa Y.; Senba E. TRPV2, a Capsaicin Receptor Homologue, Is Expressed Predominantly in the Neurotrophin-3-Dependent Subpopulation of Primary Sensory Neurons. *Neuroscience* 2005, 130, 223–228. [[PubMed](#)] [[Google Scholar](#)]
 - Tan X.-F.; Bae C.; Stix R.; Fernández-Mariño A. I.; Huffer K.; Chang T.-H.; Jiang J.; Faraldo-Gómez J. D.; Swartz K. J. Structure of the Shaker Kv Channel and Mechanism of Slow C-Type Inactivation. *Sci. Adv.*

- 2022, 8, eabm7814. [[PMC free article](#)] [[PubMed](#)] [[Google Scholar](#)]
- Togashi K.; Inada H.; Tominaga M. Inhibition of the Transient Receptor Potential Cation Channel TRPM2 by 2-Aminoethoxydiphenyl Borate (2-APB). *Br. J. Pharmacol.* 2008, 153, 1324–1330. [[PMC free article](#)] [[PubMed](#)] [[Google Scholar](#)]
 - Xu S.-Z.; Zeng F.; Boulay G.; Grimm C.; Harteneck C.; Beech D. J. Block of TRPC5 Channels by 2-Aminoethoxydiphenyl Borate: A Differential, Extracellular and Voltage-Dependent Effect. *Br. J. Pharmacol.* 2005, 145, 405–414. [[PMC free article](#)] [[PubMed](#)] [[Google Scholar](#)]
 - Yamada T.; Ueda T.; Shibata Y.; Ikegami Y.; Saito M.; Ishida Y.; Ugawa S.; Kohri K.; Shimada S. TRPV2 Activation Induces Apoptotic Cell Death in Human T24 Bladder Cancer Cells: A Potential Therapeutic Target for Bladder Cancer. *Urology* 2010, 76, 509.e1–7. [[PubMed](#)] [[Google Scholar](#)]
 - Yang F.; Vu S.; Yarov-Yarovoy V.; Zheng J. Rational Design and Validation of a Vanilloid-Sensitive TRPV2 Ion Channel. *Proc Natl Acad Sci USA* 2016, 113, E3657–66. [[PMC free article](#)] [[PubMed](#)] [[Google Scholar](#)]
 - Yang S.; Yang F.; Wei N.; Hong J.; Li B.; Luo L.; Rong M.; Yarov-Yarovoy V.; Zheng J.; Wang K.; et al. A Pain-Inducing Centipede Toxin Targets the Heat Activation Machinery of Nociceptor TRPV1. *Nat. Commun.* 2015, 6, 8297. [[PMC free article](#)] [[PubMed](#)] [[Google Scholar](#)]
 - Yao J.; Liu B.; Qin F. Kinetic and Energetic Analysis of Thermally Activated TRPV1 Channels. *Biophys. J.* 2010, 99, 1743–1753. [[PMC free article](#)] [[PubMed](#)] [[Google Scholar](#)]
 - Yao J.; Liu B.; Qin F. Modular Thermal Sensors in Temperature-Gated Transient Receptor Potential (TRP) Channels. *Proc Natl Acad Sci USA* 2011, 108, 11109–11114. [[PMC free article](#)] [[PubMed](#)] [[Google Scholar](#)]

- Zhang F.; Hanson S. M.; Jara-Oseguera A.; Krepkiy D.; Bae C.; Pearce L. V.; Blumberg P. M.; Newstead S.; Swartz K. J. Engineering Vanilloid-Sensitivity into the Rat TRPV2 Channel. *eLife* 2016, 5. [[PMC free article](#)] [[PubMed](#)] [[Google Scholar](#)]
- Zhang F.; Swartz K. J.; Jara-Oseguera A. Conserved Allosteric Pathways for Activation of TRPV3 Revealed through Engineering Vanilloid-Sensitivity. *eLife* 2019, 8. [[PMC free article](#)] [[PubMed](#)] [[Google Scholar](#)]
- Zhang K.; Julius D.; Cheng Y. Structural Snapshots of TRPV1 Reveal Mechanism of Polymodal Functionality. *Cell* 2021, 184, 5138–5150.e12. [[PMC free article](#)] [[PubMed](#)] [[Google Scholar](#)]
- Zhang L.; Simonsen C.; Zimova L.; Wang K.; Moparthi L.; Gaudet R.; Ekoff M.; Nilsson G.; Hellmich U. A.; Vlachova V.; et al. Cannabinoid Non-Cannabidiol Site Modulation of TRPV2 Structure and Function. *Nat. Commun.* 2022, 13, 7483. [[PMC free article](#)] [[PubMed](#)] [[Google Scholar](#)]
- Zheng S. Q.; Palovcak E.; Armache J.-P.; Verba K. A.; Cheng Y.; Agard D. A. MotionCor2: Anisotropic Correction of Beam-Induced Motion for Improved Cryo-Electron Microscopy. *Nat. Methods* 2017, 14, 331–332. [[PMC free article](#)] [[PubMed](#)] [[Google Scholar](#)]
- Zubcevic L.; Herzik M. A.; Chung B. C.; Liu Z.; Lander G. C.; Lee S.-Y. Cryo-Electron Microscopy Structure of the TRPV2 Ion Channel. *Nat. Struct. Mol. Biol.* 2016, 23, 180–186. [[PMC free article](#)] [[PubMed](#)] [[Google Scholar](#)]
- Zubcevic L.; Le S.; Yang H.; Lee S.-Y. Conformational Plasticity in the Selectivity Filter of the TRPV2 Ion Channel. *Nat. Struct. Mol. Biol.* 2018, 25, 405–415. [[PMC free article](#)] [[PubMed](#)] [[Google Scholar](#)]
- Zubcevic L.; Borschel W. F.; Hsu A. L.; Borgnia M. J.; Lee S.-Y. Regulatory Switch at the Cytoplasmic Interface Controls TRPV Channel Gating. *eLife* 2019, 8. [[PMC free article](#)] [[PubMed](#)] [[Google Scholar](#)]
- Zygmunt P. M.; Petersson J.; Andersson D. A.;

Högestätt E. D. Vanilloid Receptors on Sensory Nerves Mediate the Vasodilator Action of Anandamide. *Nature* 1999, **400**, 452–457. [[PubMed](#)] [[Google Scholar](#)]